

7-10-1992

Flux Trapping in Superconducting Pellets

Andreas Straub
Portland State University

Follow this and additional works at: https://pdxscholar.library.pdx.edu/open_access_etds



Part of the [Physics Commons](#)

Let us know how access to this document benefits you.

Recommended Citation

Straub, Andreas, "Flux Trapping in Superconducting Pellets" (1992). *Dissertations and Theses*. Paper 4535.

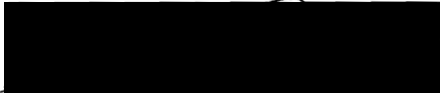
<https://doi.org/10.15760/etd.6419>

This Thesis is brought to you for free and open access. It has been accepted for inclusion in Dissertations and Theses by an authorized administrator of PDXScholar. Please contact us if we can make this document more accessible: pdxscholar@pdx.edu.

AN ABSTRACT OF THE THESIS OF Andreas Straub for the Master of Science in Physics presented July 10, 1992.

Title: Flux Trapping in Superconducting Pellets

APPROVED BY THE MEMBERS OF THE THESIS COMMITTEE:


John Dash, Chairperson


Makoto Takeo


Bruce W. Brown

This research concerns the effects on samples of nominal composition $\text{Bi}_{1.8}\text{Pb}_{0.2}\text{Sr}_2\text{Ca}_2\text{Cu}_3\text{O}_y$ which were exposed to hot, dense argon in a ballistic compressor.

The investigations were concentrated on two specimens which were exposed to hot, dense argon at about 1800 K (peak pressure 330 atm) and 1500 K (peak pressure 230 atm), respectively. Sample Bi #1 showed a completely melted surface structure after triple exposure in the ballistic compressor at 1800 K while the surface of sample Bi #7 was just partly

melted after double exposure at 1500 K.

Changes in flux trapping capability and qualitative Meissner effect were investigated in addition to the properties described by Duan, *et al.* [17,18,32], who reported changes in critical temperature, crystal structure, surface morphology and composition after exposure of samples to hot, dense argon.

After triple exposure in the ballistic compressor at a temperature of approximately 1800 K, sample Bi #1 showed an enhanced Meissner effect on the exposed side compared to the unexposed side of the pellet, while no difference in Meissner effect was found between the exposed and the unexposed side of sample Bi #7.

EDS analysis showed that both samples are inhomogeneous in chemical surface composition. Oxygen loss due to exposure to hot, dense argon could not be demonstrated.

X-ray analysis indicated that the melted surface layer of sample Bi #1 after triple exposure to hot, dense argon contains smaller crystals than before exposure in the ballistic compressor.

T_c measurements gave varying results which are explainable by the chemical inhomogeneity of the specimens.

An increase in the amount of trapped flux due to exposure of the samples to hot, dense argon could not be demonstrated.

FLUX TRAPPING IN SUPERCONDUCTING
PELLETS

by
ANDREAS STRAUB


A thesis submitted in partial fulfillment of the
requirements for the degree of

MASTER OF SCIENCE
in
PHYSICS

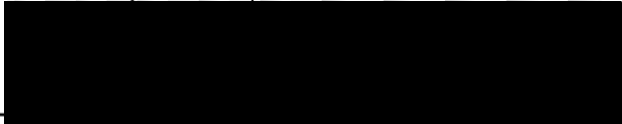
Portland State University
1992

TO THE OFFICE OF GRADUATE STUDIES:

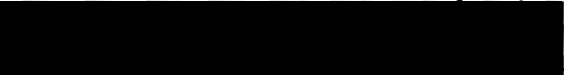
The members of the committee approve the thesis of
Andreas Straub presented July 10, 1992.

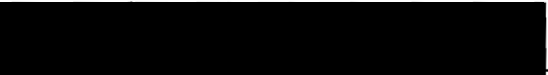

John Dash, Chairperson


Makoto Takeo


Bruce W. Brown

APPROVED:


Mark Gurevitch, Chair, Department of Physics


C. William Savery, Vice Provost for Graduate Studies and
Research

ACKNOWLEDGEMENTS

I would like to thank Dr. John Dash for giving me the possibility to complete my graduate studies in a field I was really interested in. He has given me an insight in the world of science which has helped me to see this world more clearly.

Qing Duan conducted the ballistic compressor experiments and took all the x-ray spectra. She also provided samples and introduced me to the methods she used in her work.

I will not forget many hours of discussion with Dr. Yi Pan. His comments and suggestions increased my confidence about my work.

I am grateful to Brian McLaughlin who struggled with repairing the Gaussmeter and who was always willing to lend me his expertise. He often went above and beyond the call of duty to help me.

I also wish to thank Stephen Attinasi, Rudi Zupan and Lee Thanum for their help in constructing and fixing parts which I needed in my experiments and some "special" jobs where their help was indispensable.

I am grateful to Tom Heinecke from the calibration department at Intel who provided reference magnets for the Hall probe calibration.

I would like to express a special thanks to Karl, Stephen, Catherine, Michael, Andreas and Sabine who helped

each in their own way in the completion of this work. Without their help I would have never finished this thesis in time.

It suffices to say that nothing would have been possible without the sacrifices and support of my parents.

TABLE OF CONTENTS

	PAGE
ACKNOWLEDGEMENTS	iii
LIST OF TABLES	vii
LIST OF FIGURES	x
CHAPTER	
I INTRODUCTION	1
Fundamentals	2
The Bi-Sr-Ca-Cu-O System	
High- T_c Phase (110 K) Preparation	
II PREPARATION OF Bi-Pb-Sr-Ca-Cu-O PELLETS	7
Experimental Procedure	7
Resulting Pellets	8
III THE BALLISTIC COMPRESSOR	11
Description of the PSU Ballistic	
Compressor	11
Operation and Temperature Determination	
in the Ballistic Compressor	13
Exposure of Pellets to Argon in the	
Ballistic Compressor	15
Experimental Procedure	
Results	
IV CHARACTERIZATION METHODS AND RESULTS	19
Determination of Affected	
Layer-Thickness	19

Qualitative Meissner Effect Determination	22
Experiment Discussion	
SEM Imaging	26
Sample Bi #1 Sample Bi #7 Discussion Findings of Other Researchers	
EDS Analysis	35
Qualitative Analysis Discussion Findings of Other Researchers Qualitative Analysis of Oxygen Content Discussion of Oxygen Investigation	
X-Ray Diffraction Studies	46
Indexing Discussion Crystallite Size	
T_c Measurements	61
Experiment Results Conclusions	
Flux-Trapping Measurements	69
Theory Experiment Findings of Other Researchers	
V SUMMARY AND CONCLUSIONS	76
REFERENCES	78

LIST OF TABLES

TABLE		PAGE
I	Lattice Parameters for the Three Bi-Phases (2201), (2212) and (2223) [5,9]	4
II	Final Sample Thicknesses	10
III	Maximum Temperature in the Ballistic Compressor at Different Pressure Ratios	14
IV	Qualitative Meissner Effect Measurements. The Deviation of the Magnet from the Center of the Pellet was Measured	25
V	Intensity Ratios of $Sr(L\alpha, \beta) : Bi(M\alpha, \beta) :$ $Ca(K\alpha) : Cu(K\alpha)$ Peaks. Spectra Taken from the Surface of Samples with Nominal Composition $Bi_{1.8}Pb_{0.2}Sr_2Ca_2Cu_3O_y$	35
VI	Maximal and Minimal Values of Observed Relative Peak Height for Each Element, Before and After Exposure in the Ballistic Compressor	38
VII	Intensity Ratios of $Sr(L\alpha, \beta) : Bi(M\alpha, \beta) : Ca(K\alpha) :$ $Cu(K\alpha)$ Peaks. Spectra Taken from the Surface of Sample Bi #4 Before Exposure in the Ballistic Compressor. (C) "Cornflake"-Like Particle; (1) and (2) Fiber-Like Particle	39

TABLE

PAGE

VIII	Intensity Ratios of $O(K\alpha):Cu(L\alpha,\beta)$ Peaks. Spectra were Taken From Both Sample Surfaces, (a) Unexposed Side, (b) Exposed Side and From Two Regions in the Cross-Section of the Pellet, (c) Close to the Unexposed Side and (d) Close to the Exposed Side	44
IX	X-Ray Diffraction Data for Sample Bi #1 Before and After Triple Exposure in the Ballistic Compressor	52
X	X-Ray Diffraction Data for Sample Bi #7 Before and After Double Exposure in the Ballistic Compressor	55
XI	Crystal Sizes in Sample Bi #1 Before Exposure in the Ballistic Compressor	59
XII	Crystal Sizes in Sample Bi #1 After Third Exposure in the Ballistic Compressor	59
XIII	Crystal Sizes in Sample Bi #7 Before Exposure in the Ballistic Compressor	60
XIV	Crystal Sizes in Sample Bi #7 After Second Exposure in the Ballistic Compressor	60
XV	Data of T_c Measurements Before and After Exposure of the Samples in the Ballistic Compressor (BC)	65

TABLE

PAGE

XVI	T_c Measurements by Four-Point Probe Method at Sample Bi #7 After Single Exposure in the Ballistic Compressor at Different Voltages and Currents	67
XVII	Maximum Values of Trapped Flux in Samples Bi #1 and #7 with Two Different Hall Probes	74

LIST OF FIGURES

FIGURE	PAGE
1.	The crystal structures of the Bi phases of general formula $\text{Bi}_2\text{Sr}_2\text{Ca}_{n-1}\text{Cu}_n\text{O}_y$ with $n = 1, 2$ and 3 [5] 3
2.	Diagram of the PSU ballistic compressor 12
3.	Sample mounting on the piston head 16
4.	Micrograph of the cross-section of sample Bi #1 20
5.	Enlarged image of the pore from Figure 4 21
6.	Explanation of the Meissner Effect [24] 23
7.	Qualitative Meissner Effect determination 24
8.	SEM micrographs of sample Bi #1 before exposure in the ballistic compressor 29
9.	SEM micrographs of sample Bi #1 after triple exposure in the ballistic compressor 30
10.	SEM micrographs of sample Bi #7 before exposure in the ballistic compressor 31
11.	SEM micrographs of sample Bi #7 after double exposure in the ballistic compressor 32
12.	SEM micrographs of sample Bi #7 after double exposure in the ballistic compressor 33

FIGURE	PAGE
13. EDS spectra from sample Bi #7 before (upper) and after double exposure (lower) in the ballistic compressor	36
14. SEM micrograph of sample Bi #7	37
15. SEM micrograph of the surface structure of sample Bi #4 before exposure in the ballistic compressor	40
16. EDS spectra of the fiber-like particles, marked in Figure 15 by arrow (1) (upper) and arrow (2) (lower)	41
17. EDS spectrum of the "cornflake"-like particle, marked in Figure 15 by arrow (C)	42
18. EDS spectra of sample Bi #1 of the cross- sectional area	45
19. Standard four-point probe configuration	62
20. Resistance of sample Bi #1 vs. temperature before (a) and after triple exposure (b) in the ballistic compressor	66
21. Phase diagram of a Type II superconductor [24]	70
22. Magnetization of a Type II superconductor [36]	72

CHAPTER I

INTRODUCTION

In 1986 J.G. Bednorz and K.A. Müller discovered high transition temperatures (T_c) of about 30 K in the superconducting system $Ba_xLa_{5-x}Cu_5O_{5(3-y)}$ [1].

This stimulated an intensive worldwide search for materials with even higher transition temperatures.

In the beginning of 1987 Wu, *et al.* [2] achieved a transition temperature of $T_c = 90$ K in the system $YBa_2Cu_3O_7$,

Michel, *et al.* [3] reported a T_c of about 14 K for the system Bi-Sr-Cu-O in the same year.

The break through to high- T_c superconductivity with transition temperatures above 100 K was accomplished by Maeda, *et al.* [4] in early 1988.

The addition of Ca in the Bi-Sr-Cu-O system led Maeda, *et al.* [4] to the discovery of bulk superconductivity at 85 K and evidence of superconductivity at 110 K in the Bi-Sr-Ca-Cu-O system.

FUNDAMENTALS

The Bi-Sr-Ca-Cu-O System

Today it is known that there are three superconducting phases having the general formula $\text{Bi}_2\text{Sr}_2\text{Ca}_{n-1}\text{Cu}_n\text{O}_y$ with $n = 1, 2,$ and 3 [5,6]. The $n = 1$ phase, with composition $\text{Bi}_2\text{Sr}_2\text{CuO}_y$ (2201), shows superconductivity at 10 K, while the $n = 2$ phase, $\text{Bi}_2\text{Sr}_2\text{CaCu}_2\text{O}_y$ (2212), and the $n = 3$ phase, $\text{Bi}_2\text{Sr}_2\text{Ca}_2\text{Cu}_3\text{O}_y$ (2223), demonstrate superconductivity at 85, and 110 K, respectively [5]. Usually bulk specimens are mixtures of all three phases. The preparation of single-phase high-temperature superconducting materials based on Bi is still a problem [7].

The crystal structures of the three phases are similar, as shown in Figure 1, differing only in the number of CuO_2 -Ca- CuO_2 slabs packed along the c axis. The structure can be described as a stacking of a basic $\text{Bi}_2\text{Sr}_2\text{CuO}_6$ unit, where one layer of Cu-O is sandwiched between two layers of Sr-O and two layers of Bi-O. For the (2201), (2212), and (2223) phase, respectively, either zero, one, or two CaCuO_2 slabs, consisting of one Ca layer and one CuO_2 layer are inserted [5]. T_c increases with an increasing number of CaCuO_2 slabs as n increases from one to three, but decreases for further increases of n ($n > 3$) [8].

A common characteristic of all three phases is the presence of two Bi-O layers separated by 3.0 Å [5] and shifted, with respect to each other (crystallographic shear)

along the diagonal direction of the perovskite subcell. The structure is described as pseudotetragonal, with $a=b= 5.4 \text{ \AA}$. The c lattice parameter increases from 24.4 to 30.76 [9] and then to 37.1 \AA [5], respectively, in going from the $n = 1$ to $n = 2$ and $n = 3$ phase. This increase results from the progressive addition of CaCuO_2 to the stacking sequence in the unit cell [5]. The volume per atom in the unit cell decreases with increasing number of n .

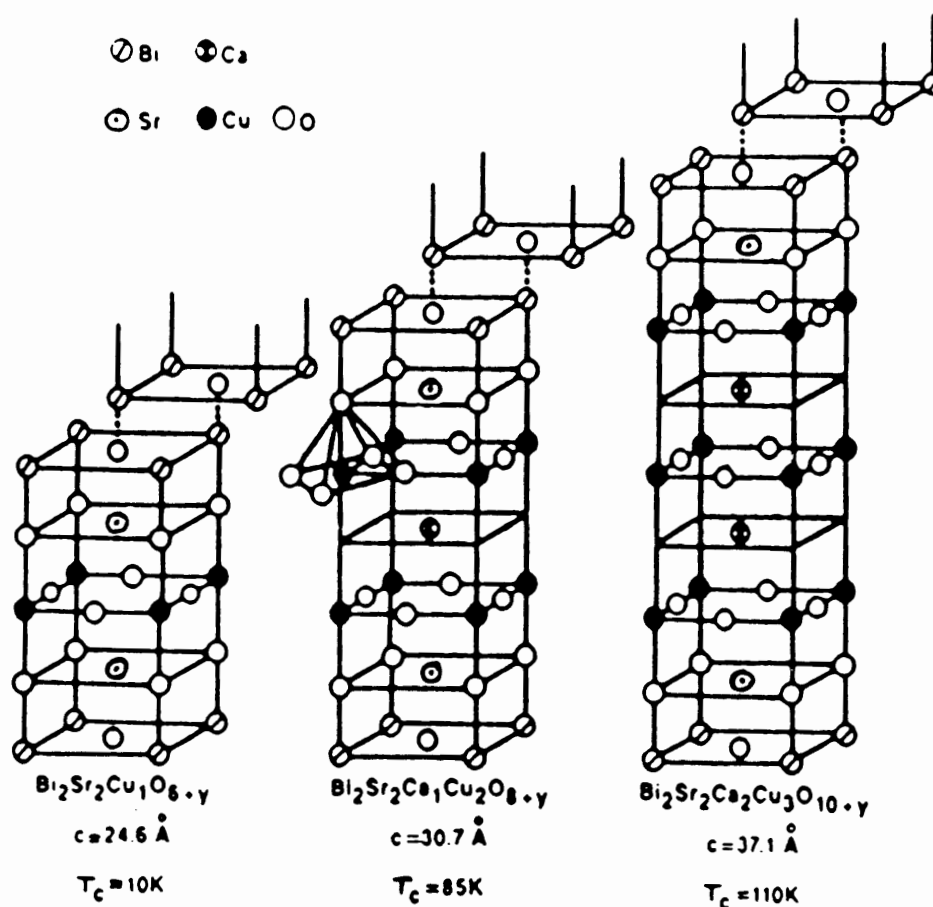


Figure 1. The crystal structures of the Bi phases of general formula $\text{Bi}_2\text{Sr}_2\text{Ca}_{n-1}\text{Cu}_n\text{O}_y$ with $n = 1, 2$ and 3 [5].

TABLE I
LATTICE PARAMETERS FOR THE THREE BI-PHASES
(2201), (2212) AND (2223) [5,9]

	(2201) $T_c=10$ K	(2212) $T_c=85$ K	(2223) $T_c=110$ K
a, b	5.4 Å	5.4 Å	5.4 Å
c	24.4 Å	30.76 Å	37.1 Å

High- T_c Phase (110 K) Preparation

The multiphase character of the materials, based on Bi is well known [5-8]. Difficulties have been encountered in the preparation of single-phase materials based on Bi. Particularly unstable is the (2223) phase with $T_c = 110$ K [5-8], which is also the most interesting phase, because of its high transition temperature.

The contribution of a particular phase to the material depends strongly on the initial stoichiometry, but depends also on other factors. It has been reported that the partial substitution of Bi by Pb can either stabilize or favor the formation of the 110 K phase [10,11]. This beneficial effect was confirmed by several other investigators [6-8,10-13]. Doping of the material by Pb leads to a stabilization of the 110 K phase, but does not affect the lattice constants shown in Table I.

In a systematic investigation of the effect of Pb-doping on the $\text{Bi}_{2-x}\text{Pb}_x\text{Sr}_2\text{Ca}_2\text{Cu}_3\text{O}_y$ system, the highest T_c values, and therefore the largest amounts of the (2223) phase with respect

to the two other phases, (2201) and (2212), were obtained for x values between 0.2 and 0.3 [6]. The reason for the stabilizing effect of Pb-doping as well as the exact lattice sites at which Pb is substituted are not known yet.

Another important factor, which is independent from Pb-doping, to obtain a large percentage of (2223) phase with respect to the two other phases, (2201) and (2212), is the sample processing, in particular, the annealing time, and temperature as well as the cooling rates of the samples [5,6,7,10,13,14].

Annealing times for the material between several hours and up to 350 hours [6] were performed. Annealing for longer than 100 hours does not yield any significant changes [6].

Between different processes, the samples are reground and recompact several times in order to obtain a better homogeneity [6]. Preheating processes at lower temperatures of about 770 °C avoid partial melting in the following sintering processes, where the temperature is higher [6].

In general, a higher annealing temperature produces a higher T_c [5], but higher temperatures also increase the risk that one constituent could be lost. Experimentally it was shown that, depending upon whether the sample is heated below or above its melting point (885 °C for the (2223) phase), there are considerable differences in the resulting properties [5]. Changing the annealing temperature by only 10 °C was enough to change the T_c of the resulting material by 15 K [5].

This behavior can be explained by stacking faults, which are common in layered materials [5]. In these faults some layers of the n phase are replaced by the $n-1$ or $n+1$ phase, for example layers of $\text{Cu}_3\text{Ca}_2\text{O}_6$ from the (2223) phase are replaced by layers of Cu_2CaO_4 from the (2212) structure. The removal of these stacking faults depends on the annealing temperature and time, which are hence important parameters in sample processing [5]. The cooling rate is also important for growing the desired phase [5,14].

The most systematic effort to investigate the appropriate thermal procedure as well as the optimal percentage of Pb for the preparation of the $\text{Bi}_{2-x}\text{Pb}_x\text{Sr}_2\text{Ca}_2\text{Cu}_3\text{O}_y$ phase (Pb-doped (2223) phase) was made by Pissas, *et al.* [6]. The highest T_c values and hence largest amount of the (2223) phase with respect to the two other phases, (2201) and (2212), were obtained for x values between 0.2 and 0.3 and a final sintering temperature between 860 - 875 °C [6].

However, even higher temperatures and cooling rates might favor the formation of the high- T_c 110 K phase, and hence increase the transition temperature of the samples.

The PSU ballistic compressor, which is described later, is a unique apparatus capable of producing gases at temperatures as high as 6000 K for about half a millisecond and cooling rates as high as 10^5 °C per second [15].

CHAPTER II

PREPARATION OF Bi-Pb-Sr-Ca-Cu-O PELLETS

This chapter describes the preparation of bulk polycrystalline samples with possible T_c values of about 100 K. In the system Bi-Pb-Sr-Ca-Cu-O this is only possible by partial substitution of Bi by Pb, which was first reported by Sunshine, *et al.* [16]. In their work, they note that the T_c of a multiphase Pb-doped sample was raised from 84 K to 100 K.

EXPERIMENTAL PROCEDURE

Sintered samples of nominal composition $\text{Bi}_{1.8}\text{Pb}_{0.2}\text{Sr}_2\text{Ca}_2\text{Cu}_3\text{O}_y$ were prepared by solid-state reaction. Appropriate amounts of bismuth oxide, Bi_2O_3 , (min. 99% pure; EM Science Inc., Cherry Hill), lead oxide, Pb_3O_4 , (99.5% pure; J.T. Baker Chemical Co., Phillipsburg), calcium carbonate, CaCO_3 , (99.95% - 100.05% pure; Mallinckrodt Inc., Kentucky), strontium carbonate, SrCO_3 , (min. 98.5% pure; Allied Chemical, New York), and copper oxide, CuO , (99.5% pure; J.T. Baker Chemical Co., Phillipsburg) were well mixed and ground in a mortar and pestle. CaCO_3 was preheated for two hours at 200 °C to drive out possible water content. The powder mixture was calcined in air at 800 °C for 16 hours. The resulting powder block was

reground and pressed into 22 disc-shaped pellets of 0.5 inch diameter at a pressure of 10,000 psi and a temperature of about 100 °C. The thickness of the pellets varied between 0.8 mm and 2.5 mm, where 0.625 g powder correspond to approximately 1 mm resulting sample thickness.

Subsequently, the pellets, standing on the edges, were put in a tube of mullite, calcined in air at 865 °C for 60 hours, and then quenched in liquid nitrogen.

This method was applied successfully before [17,18]. The observed temperature highpoint was 893 °C. This is in a range, where liquid and solid material co-exist [19]. The observed lowpoint was 839 °C.

RESULTING PELLETS

Due to the exceeding of the temperature where the material is solely solid, some pellets were baked together and had to be separated by means of a razor blade, while others lost their original shape and were either thicker on the bottom edge, due to the standing position in the oven, or they were bent. The thin pellets (0.8 mm thickness) especially were affected by bending. Only 12 of the 22 pellets were useable. Five pellets were baked together and broke apart when separation was attempted and the remaining five showed almost no Meissner effect, which is described later in detail. The material resulting from the heating and quenching is very brittle and behaves like a ceramic.

The 12 useable pellets showed different surface appearances, depending on whether the surface was directly in contact with air (smooth, shining, glass-like surface) or if the pellet was in contact with the neighbor-pellet during the heating process (rough, lusterless surface).

This difference was also visible in the strength of observed Meissner effect. A cylindrical neodymium magnet (1 mm in diameter, 1 mm long) was placed on the surface of the pellets at liquid nitrogen temperature. Its repulsion was visibly stronger from the edges of the pellets, while it was sometimes not repelled at all when placed directly in the center of the pellets.

Out of the 12 useable pellets, six specimens (Bi #5 to #10 in Table II) were chosen for the present investigation. These showed almost homogeneous repulsion of the magnet across the whole surface.

To prevent breaking of the brittle material in further treatments, like exposure in the ballistic compressor and T_c measurements, it was necessary to regain a planar surface. This was accomplished by sanding the samples with 600 mesh sandpaper until flatness and roundness was restored.

Samples Bi #1 to #4 were produced, following the same process, by Q. Duan, Department of Physics, Portland State University.

Table II gives an overview for the thicknesses of samples after sanding, which were used for further investigations.

TABLE II
FINAL SAMPLE THICKNESSES

Sample Number	Thickness in mm
Bi #1	3.2
Bi #2	2.9
Bi #3	1.6
Bi #4	1.3
Bi #5	0.6
Bi #6	0.6
Bi #7	0.8
Bi #8	1.1
Bi #9	0.9
Bi #10	0.9

CHAPTER III

THE BALLISTIC COMPRESSOR

DESCRIPTION OF THE PSU BALLISTIC COMPRESSOR

The ballistic compressor at Portland State University is a modification of the original structure, which has already been fully described elsewhere [20]. A brief description of the present device has also been published [15].

As shown in Figure 2a, the compressor consists of a horizontally mounted 2.90 m long, 5.715 ± 0.003 cm inner diameter tube (A) attached on one end to the driving-gas reservoir (B) and on the other to the high pressure head (C). With a 52.63 cm long, 9.63 kg piston in prefiring position, the volume of the driving-gas reservoir is 10.57 liters, and the volume of the test-gas chamber is 7.5 liters. The maximum possible stroke is 2.77 m.

The high-pressure head, shown in Figure 2b, is made from ARMCO 17-4 PH stainless steel 25 cm in diameter, which is able to withstand a gas pressure of 6000 atm.

The driving-gas reservoir, shown in Figure 2c, contains the piston-holding and -release mechanism. In the prefiring position, the tail of the piston (D) extends through the driving-gas reservoir (B) into a chamber (E) in which a pair of spring-loaded jaws (F) latches around a nub attached to the

rear of the piston. Piston release is accomplished by the forward motion of a plunger (G) which opens the springloaded jaws and pushes the piston out of the chamber.

The piston is shown in Figure 2d. The piston head (H) has a diameter of 0.05 mm less than the bore of the tube, and is made from the same material as the high-pressure head. The bronze piston rings (I) are grooved to reduce gas leakage during the compression stroke. Three Teflon runners (J) center the piston in the compressor bore. In the prefiring position, the raised portion (K) of the piston-body compresses a pair of O-rings in the front of the driving-gas reservoir isolating the test-gas from the driving-gas.

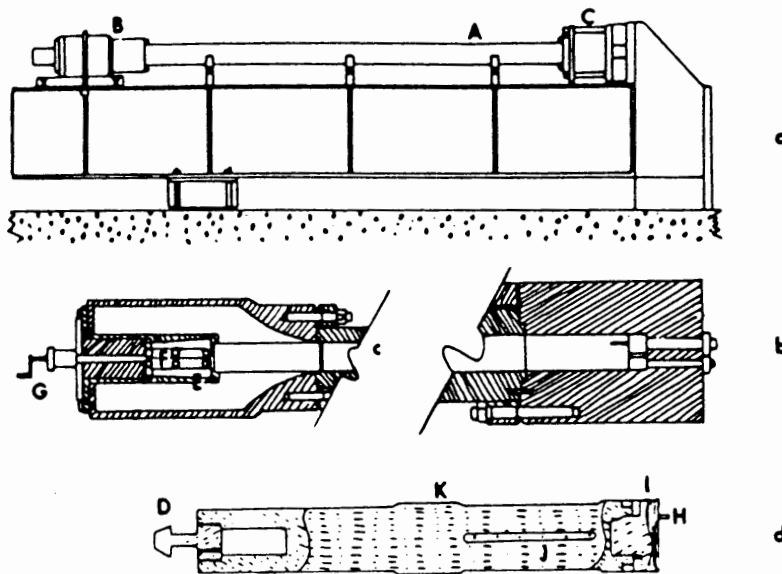


Figure 2. Diagram of the PSU ballistic compressor. (a) Side view of the horizontally mounted free-piston compressor; (b) A pressure transducer is mounted at an end of the side wall of the high-pressure head; (c) The piston holding- and release-mechanism are housed within the driving-gas reservoir; (d) The 9.63 kg piston [15].

OPERATION AND TEMPERATURE DETERMINATION
IN THE BALLISTIC COMPRESSOR

In operation, the piston is released by the mechanism described before and accelerated down the bore by the pressure gradient between driving-gas reservoir and test-gas chamber. The piston moves back and forth several times before friction brings it to rest.

A PCB Piezotronics Model 105A pressure transducer is mounted at an end of the side wall of the high-pressure head. The output of the pressure transducer is recorded on an oscilloscope (Tektronix RM35A) by means of a Polaroid camera. The peak pressure at each firing can thus be read on the oscillogram.

The minimum distance of the piston head from the back wall of the test-gas chamber was determined by means of a copper wire, which was mounted in one of the bores of the piston head. The wire was bent when it was pushed against the back wall of the test-gas chamber. The minimum distance was determined directly by measuring the length of the bent wire. The flexibility of the wire was reduced by annealing, to avoid falsification of the measured lengths.

The gas temperature was found by using a computer program as described in detail elsewhere [20]. The program solves the equation of motion for the piston, with allowance for heat loss of the test gas by conduction through the compressor wall and gas leakage through the piston gap. The friction is

estimated from the viscous flow of leaking gas, allowing for the temperature dependence of the viscosity.

The parameters for the radial clearance of the piston gap and the heat conduction constant, used in the computer program, were adjusted such that the computed peak pressure (P_c) and minimum distance (D_c) agreed with the experimentally determined values (P_{exp} , D_{exp}). In this case, the temperature was also given by the computer program. Initial pressure ratios between driving-gas reservoir and test-gas chamber of 350 psi: 1 atm and 300 psi : 1 atm, respectively, have been used. The resulting maximum temperatures as well as the fit of the experimental with the computed data are shown in Table III.

The cooling rate of the gas in the rebounding stroke is as fast as 10^5 °C per second.

TABLE III
MAXIMUM TEMPERATURE IN THE BALLISTIC COMPRESSOR
AT DIFFERENT PRESSURE RATIOS

Ratio	D_{exp}	D_c	P_{exp}	P_c	T
350psi/1atm	6.6cm	6.6cm	336.0atm	335.9atm	1834 K
300psi/1atm	7.5cm	7.5cm	232.8atm	233.0atm	1504 K

In the present thesis the ballistic compressor has been used to study effects on superconducting specimens caused by the rapid heating and cooling process taking place during compressor operation.

EXPOSURE OF PELLETS TO ARGON IN THE BALLISTIC COMPRESSOR

Originally the ballistic compressor was developed to generate a hot, dense gas to investigate pressure broadening of spectral lines [21].

Later, the apparatus was used to study effects on materials which were exposed to hot, dense argon [15].

The importance of the thermal treatment in the sample preparation of high- T_c superconductors was described before in this thesis. High temperatures and rapid cooling were reported to be especially beneficial in stabilizing the high- T_c 110 K phase in the multiphase system Bi-Pb-Sr-Ca-C-O [5].

Since the Portland State University ballistic compressor is capable of producing gases at temperatures as high as 6000K and cooling rates as high as 10^5 °C per second, it offers unique capabilities to investigate the effects on samples of the Bi compound caused by the rapid heating and cooling process, taking place during compressor operation.

The investigated samples were characterized before and after exposure in the ballistic compressor by means of Meissner effect, surface structure and composition, x-ray diffraction, T_c determination, and flux trapping capability.

Experimental Procedure

Samples were mounted on the piston head by using either an annular metallic holder screwed onto the piston head, or by using double stick tape. The samples had to be mounted on the

solid part of the piston, not over one of the screw bores, to avoid breaking of the samples due to pressure differences in the hole behind the pellet and the test gas area.

When using the annular holder, usually several thin metal discs had to be put underneath the pellets, to guarantee a tight mounting on the piston head, as shown in Figure 3.

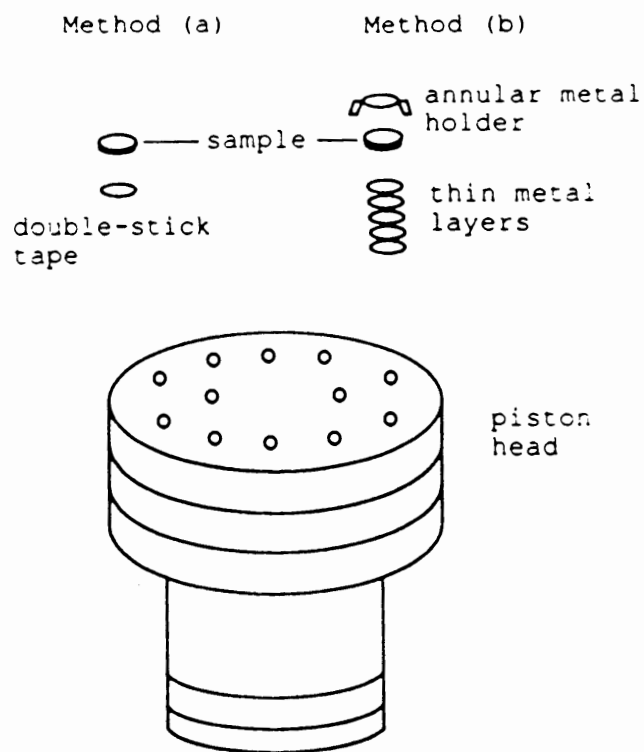


Figure 3. Sample mounting on the piston head. (a) by double stick tape, or (b) an annular metal holder.

The driving-gas as well as the test-gas in these studies were always pure argon (99.997% pure). Before the final process of firing, the ballistic compressor was flushed five

or six times with argon to avoid any air contamination. Before firing, there was a delay of about 30 minutes for the test-gas to reach room temperature. The initial pressure ratio between driving-gas reservoir and test-gas chamber was at first 350 psi : 1 atm, later it was lowered to 300 psi : 1 atm. After exposure to hot, dense argon, the samples were unscrewed from the piston head or taken off by means of a razor-blade, depending on the mounting method.

Results

The Bi compound material is brittle and the pellets are easy to break. Both mounting methods turned out to be unsatisfactory for this material, because all pellets broke.

Sample Bi #1, which was mounted with the annular metallic holder, broke during the third exposure in the ballistic compressor into two halves. SEM imaging showed that the surface of the sample was completely melted.

Samples Bi #2 and #3, which were mounted in exactly the same way, broke during the first exposure.

After changing to the double-stick tape mounting method, samples Bi #4, #8 and #10 broke into several pieces during the first exposure.

Thereafter, the pressure in the driving-gas reservoir was lowered to 300 psi. Sample Bi #7 broke during the second exposure in the ballistic compressor in two halves, where both exposures were performed with the lowered pressure of 300 psi. SEM imaging reveals, that the surface of sample Bi #7 was not

completely melted.

Other mounting methods were even worse. Foamy double-stick tape, which should have acted as a shock absorbing medium between pellet and piston head just melted away due to the high temperatures, resulting in detachment of the pellet from the piston head.

The breaking of the pellets might occur due to three main reasons: a. thermal stress due to the temperature gradient in the pellet, b. there are possible pressure differences between the test-gas area and the space between double-stick tape or back side of the pellets and piston head, c. the mechanical shock due to small notches in the inner compressor wall [22], and d. turbulent shock waves in the gas [22]. The mechanical shock could probably be absorbed by improved mounting methods, while thermal stress is unavoidable in this process. Breaking due to pressure differences is also very likely, since the gas flows slowly in and out behind the pellet; the pressure differences can be very high [22].

Two samples were exposed in the ballistic compressor more than one time. Sample Bi #1 has a completely melted surface structure after three exposures at approximately 1800 K, while sample Bi #7 still shows some features of the original structure after two exposures at approximately 1500 K. The temperature, which is necessary to melt the pellet surface completely, is not achieved with the lowered firing pressure ratio of 300 psi : 1 atm.

CHAPTER IV

CHARACTERIZATION METHODS AND RESULTS

DETERMINATION OF AFFECTED LAYER-THICKNESS

The determination of the cross-sectional area, which is affected by the hot, dense gases, is a problem, since no definite criterion was found to answer this question clearly.

The hot, dense gases are expected to melt the material up to a certain depth. Below this depth the particles in the material are expected to show rounded edges and finally the unaffected particles occur. This transition was not observed. Even at high magnifications, SEM imaging does not reveal a clear transition between affected and unaffected layers.

Since these polycrystalline bulk specimens are highly inhomogeneous in chemical composition, as shown later, locally applied EDS analysis has to be ruled out as an applicable tool in differentiating between affected and unaffected layer.

The sample surfaces are porous. With increasing number of exposures in the ballistic compressor, these pores become more and more obvious. The hot, dense gases penetrate into the pores and melt the material inside the pores.

In Figure 4 (left side), arrow (1) marks the exposed surface of sample Bi #1, after triple exposure in the ballistic compressor, and arrow (2) marks the cross-section of

the pellet. Arrow (3) indicates the edge between sample surface and cross-section. Figure 4 (right side) is a ten times enlarged micrograph of the pore located on the edge. Figure 5 is a further enlarged micrograph of the pore, which has a depth of approximately $220\ \mu\text{m}$. The image shows clearly that the inner surface of the pore looks smooth and melted, which gives proof of hot, dense gas penetration into the pores.



Figure 4. Micrograph of the cross-section of sample Bi #1. (1) is the exposed surface of the sample, (2) the cross-sectional area, (3) indicates the edge between exposed surface and cross-section.

Hence, the maximum penetration depth of the hot, dense gases is in the order of a few $100\ \mu\text{m}$. Disregarding the pores, the "real" penetration depth into the material is far less.

The edges of the pore in Figure 5 are bright, which

indicates electrical charging of the sample. This is very common for melted material of this compound which is often not electrically conducting. Measuring the thickness of the bright edge yields a "real" affected surface layer thickness of about 5 to 10 μm . This is a reasonable value, however, it remains a rough estimation, which is in correspondence with [23].



Figure 5. Enlarged image of the pore from Figure 4. The affected layer thickness was estimated from the bright edge of the pore on the right side.

QUALITATIVE MEISSNER EFFECT DETERMINATION

The behavior of a superconductor in a magnetic field (B) can not solely be explained by its infinite electrical conductivity. There is an additional property of the superconducting state. This is explained in Figure 6.

Placing a superconducting specimen in a magnetic field (B) after cooling it below its critical temperature (T_c) causes the induction of permanent electrical surface currents [24]. The magnetic field of these currents shields the volume of the superconductor from the external applied magnetic field (B); see Figure 6a.

On the other hand, placing the superconductor in a magnetic field (B) at room temperature yields quick attenuation of the induced currents, resulting in penetration of the specimen by the magnetic field (B). Considering an infinite conductivity as the only property of a superconductor this state should not change with subsequent cooling below T_c of the specimen; see Figure 6b. Comparison with Figure 6a would yield distinct final states of the superconductor, depending on whether the sample was first cooled and subsequently placed in a magnetic field or vice versa. The properties of the specimen in the superconducting state would depend on the "way" the specimen became superconducting.

In 1933, W. Meissner and R. Ochsenfeld [25] showed, that the result is independent of the "way" in the experiment and

yields always the situation shown in Figure 6c, i.e. the volume of the superconductor is shielded from the magnetic field (B). This phenomenon is known as the Meissner-Ochsenfeld effect (hereafter denoted as Meissner effect). The Meissner effect is the second property, besides infinite conductivity, which characterizes superconductors in the superconducting state.

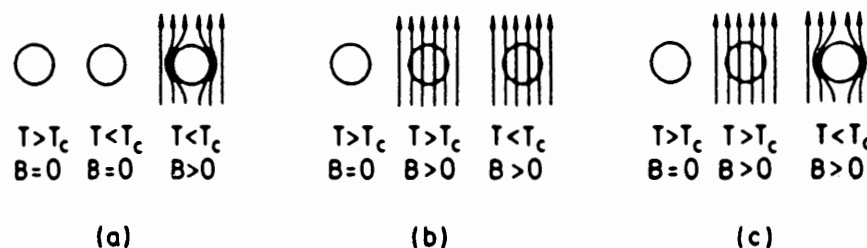


Figure 6. Explanation of the Meissner effect [24].

Experiment

The Meissner effect is demonstrated by the suspension ($\text{YBa}_2\text{Cu}_3\text{O}_7$) or repulsion (Bi compounds) of a small magnet, when placed on a specimen in the superconducting state.

The experimental setup for qualitative Meissner effect determination is shown in Figure 7. A small magnet (0.2 g) of irregular shape, which caused a magnetic field of about 30 Gauss on the pellet surface, was attached to a long thread, which was hooked on a stand. The specimens were secured by means of double-stick tape to the bottom of a styrofoam cup to prevent them from moving. Thereafter the magnet was placed approximately 1 mm above the center of the pellet. Subsequent

cooling of the specimen with liquid nitrogen caused repulsion of the magnet. The deviation of the magnet from the center position of the pellet was measured by means of a ruler, and is a measure of the strength of the Meissner effect.

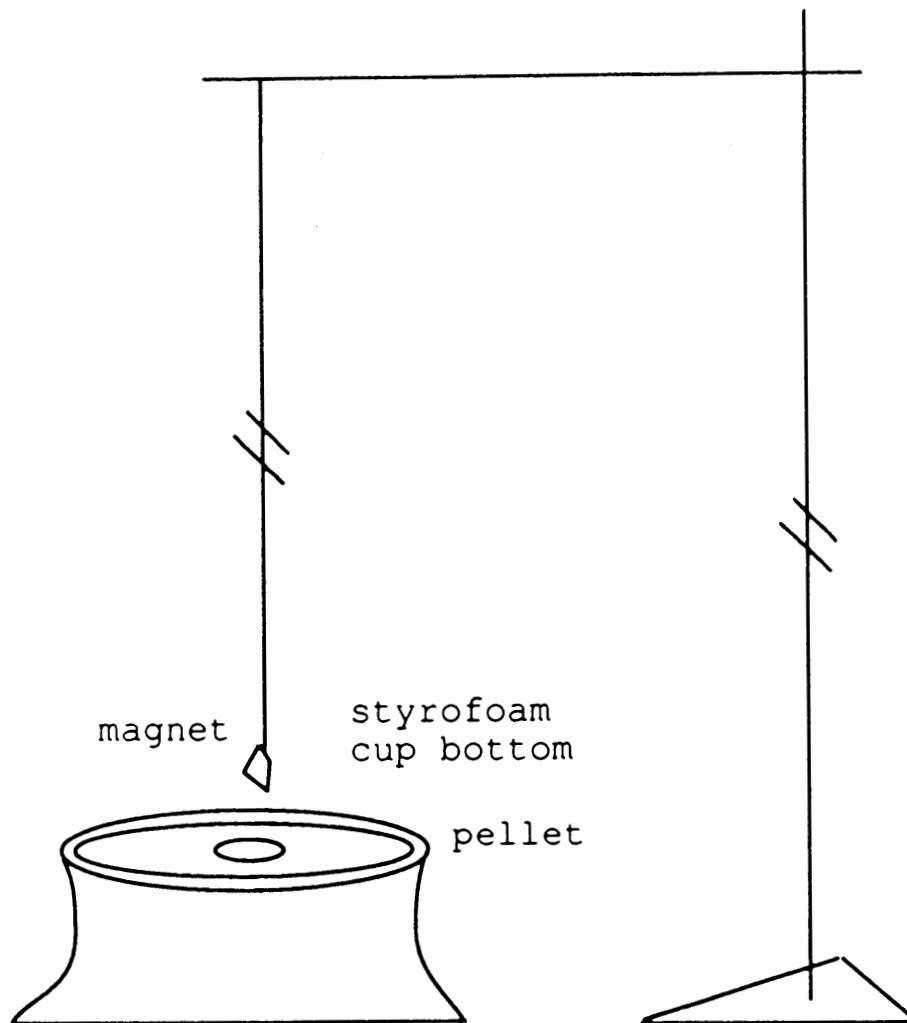


Figure 7. Qualitative Meissner effect determination.

Since the shape of the magnet is irregular, it had to be ascertained that the repulsion occurred always in the same direction when measuring the deviation of the magnet, to avoid wrong results due to irregularities in the shape of the

magnet. The specimens were tested on the exposed and on the unexposed side, respectively. Results are given in Table IV.

TABLE IV
 QUALITATIVE MEISSNER EFFECT MEASUREMENTS.
 THE DEVIATION OF THE MAGNET FROM THE
 CENTER OF THE PELLET WAS MEASURED

Sample Number	Exposed Side	Unexposed Side
Bi #1, 3 x BC 3.2 mm thick	5.0±0.5 mm	3.0±0.5 mm
	4.5±0.5 mm	3.0±0.5 mm
	4.5±0.5 mm	3.0±0.5 mm
	4.5±0.5 mm	3.0±0.5 mm
Bi #7, 2 x BC 0.8 mm thick	7.0±0.5 mm	7.0±0.5 mm
	7.0±0.5 mm	8.0±0.5 mm
	7.0±0.5 mm	7.0±0.5 mm
	7.0±0.5 mm	7.0±0.5 mm
Bi #4, 1 x BC 1.3 mm thick	9.5±0.5 mm	9.0±0.5 mm
	9.0±0.5 mm	9.0±0.5 mm
	9.0±0.5 mm	9.0±0.5 mm
	9.0±0.5 mm	9.0±0.5 mm

Discussion

Sample Bi #1 shows a clear enhancement in Meissner effect on the exposed side compared to the unexposed side, while samples Bi #4 and #7 show the same strength in Meissner effect on both sides.

Samples Bi #4 and #7 are both thin samples (1.3 mm and 0.8 mm, respectively), with a partly melted surface structure, while sample Bi #1 is a thick sample (3.2 mm), with a

completely melted surface structure.

The result indicates that the melting of the material yields an increase in Meissner effect. However, considering the absolute values, both samples Bi #4 and #7 show higher deviations of the magnet on both sides, and hence stronger Meissner effect, than sample Bi #1.

SEM IMAGING

Before and after exposure in the ballistic compressor, samples Bi #1 and #7 were examined under an SEM (ISI SS40).

Each of Figures 8 to 12 display two micrographs. The upper images are dual-magnification images at magnifications of 50X (left side) and 500X (right side), respectively. The lower micrographs are further enlargements of the same area and were taken at a magnification of 1000X. The arrows in the images mark corresponding features.

The top electron detector of the SEM had to be switched off when the low-magnification micrographs were taken, otherwise a bright spot occurred in the middle of the image. Therefore, with the top electron detector, the 1000X micrographs reveal a more detailed morphology of the sample surface.

Figures 8 and 10 illustrate the porous microstructure of samples Bi #1 and #7, respectively, before exposure to hot, dense argon in the ballistic compressor. The micrographs display a granular structure with a "cornflake"-like

appearance. The particle size of the larger "cornflakes" is determined to about 5 μm . Fiber-like particles among the larger particles of about 5 μm length are also found.

The upper micrographs in both figures also illustrate the porosity of the surface.

A special feature, shown in Figure 10, are flutes, which are due to the treatment with sandpaper. The lower image shows that some of the particles are randomly oriented, while others are arranged in regular layers. The edges of the grains are sharp and distinguishable, as shown at the marked edge.

The effect on the two samples, due to the exposure to hot, dense argon in the ballistic compressor, is apparently distinct.

Sample Bi #1

Figure 9 shows the surface structure of sample Bi #1 after triple exposure in the ballistic compressor, at a pressure ratio between driving-gas reservoir and test-gas chamber ratio of 350 psi : 1 atm. The image suggests that surface melting has occurred. The sample surface is interspersed with trenches and is partly melted away, as shown in the 50X micrograph.

The search for remaining fragments of the structure before exposure in the ballistic compressor is expected to be successful in the identifiable rough areas, which are not apparently melted. However, the lower image of Figure 9 shows a melted structure even in those regions of the surface.

Sample Bi #7

The 50X micrographs in Figures 11 and 12 display an identical area of the sample surface after double exposure in the ballistic compressor, at a pressure ratio between driving-gas reservoir and test-gas chamber of 300 psi : 1 atm. The enlarged areas, however, are apparently different. Figure 11 illustrates a completely melted part of the surface, while Figure 12 shows another part, about 250 μm away from that in Figure 11, which is much less affected by the rapid heating and cooling process. The granular structure is still present, but the edges of the particles are rounded and appear particularly bright on the image. As mentioned before, this indicates charging of the material and is typical of melted Bi compound features.

Discussion

Figure 9 suggests that surface melting has occurred. Even the rough areas of the sample surface of Bi #1 are melted. Fragments of the structure before exposure in the ballistic compressor are not found after triple exposure to hot, dense argon at a temperature of 1804 K; see Table III.

Figures 11 and 12 reveal that the sample surface of Bi #7 after double exposure in the ballistic compressor at a temperature of about 1500 K (Table III) is only partly melted. Large areas of the original, granular morphology are still present in the surface. The temperature of about 1500 K is not high enough to melt the sample surface completely.

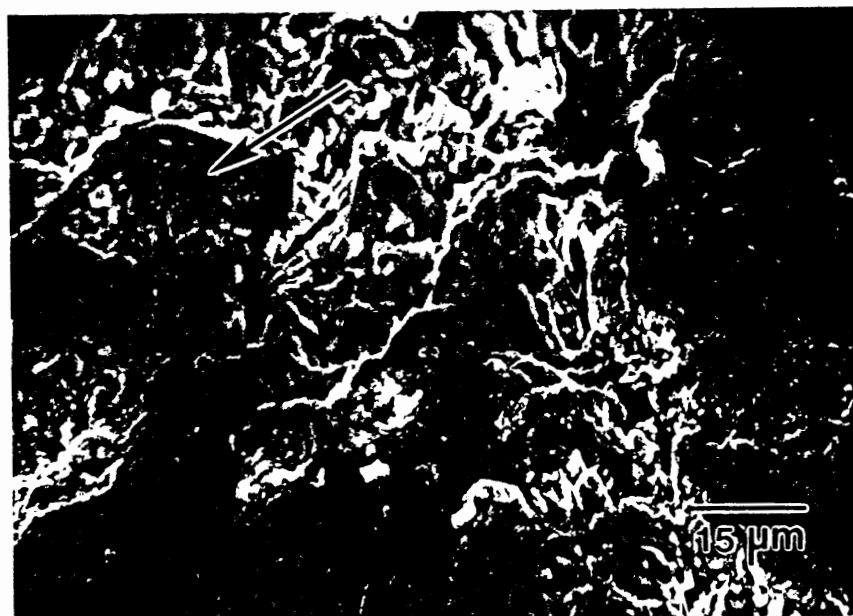
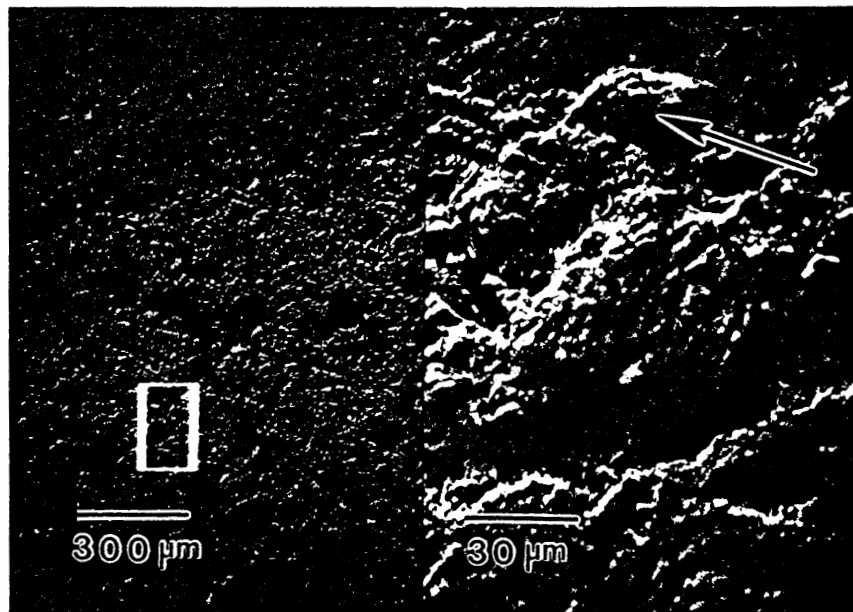


Figure 8. SEM micrographs of sample Bi #1 before exposure in the ballistic compressor. The surface shows a granular structure. The arrows mark corresponding features.

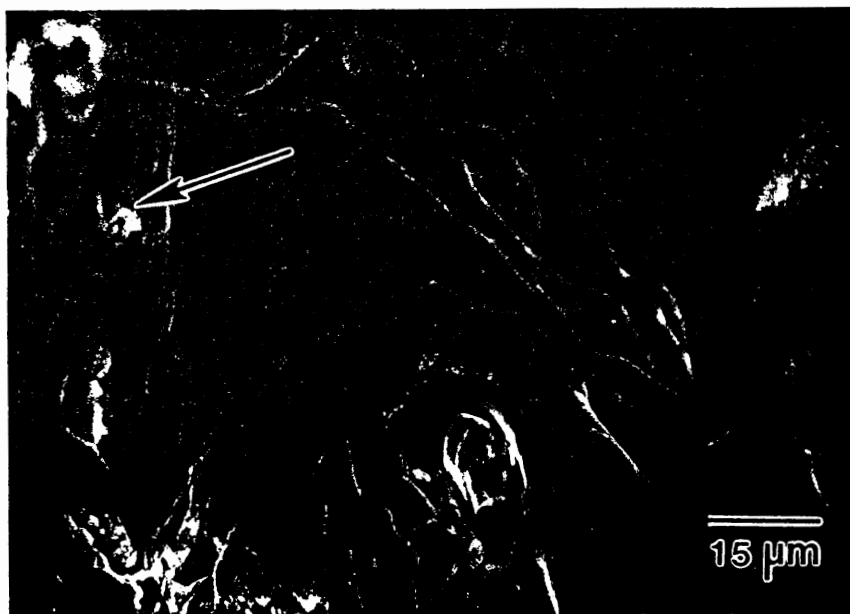
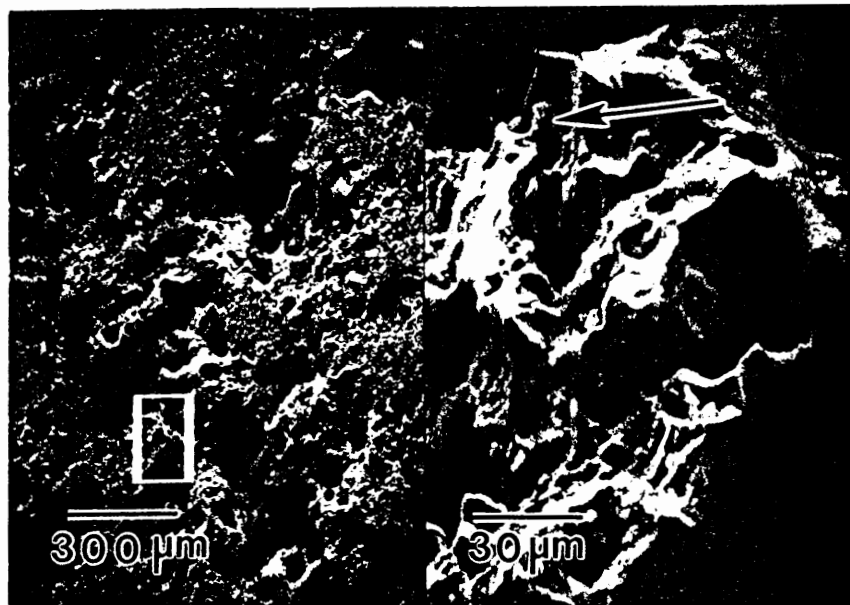


Figure 9. SEM micrographs of sample Bi #1 after triple exposure in the ballistic compressor. The images indicate that surface melting has occurred. The arrows mark corresponding features.

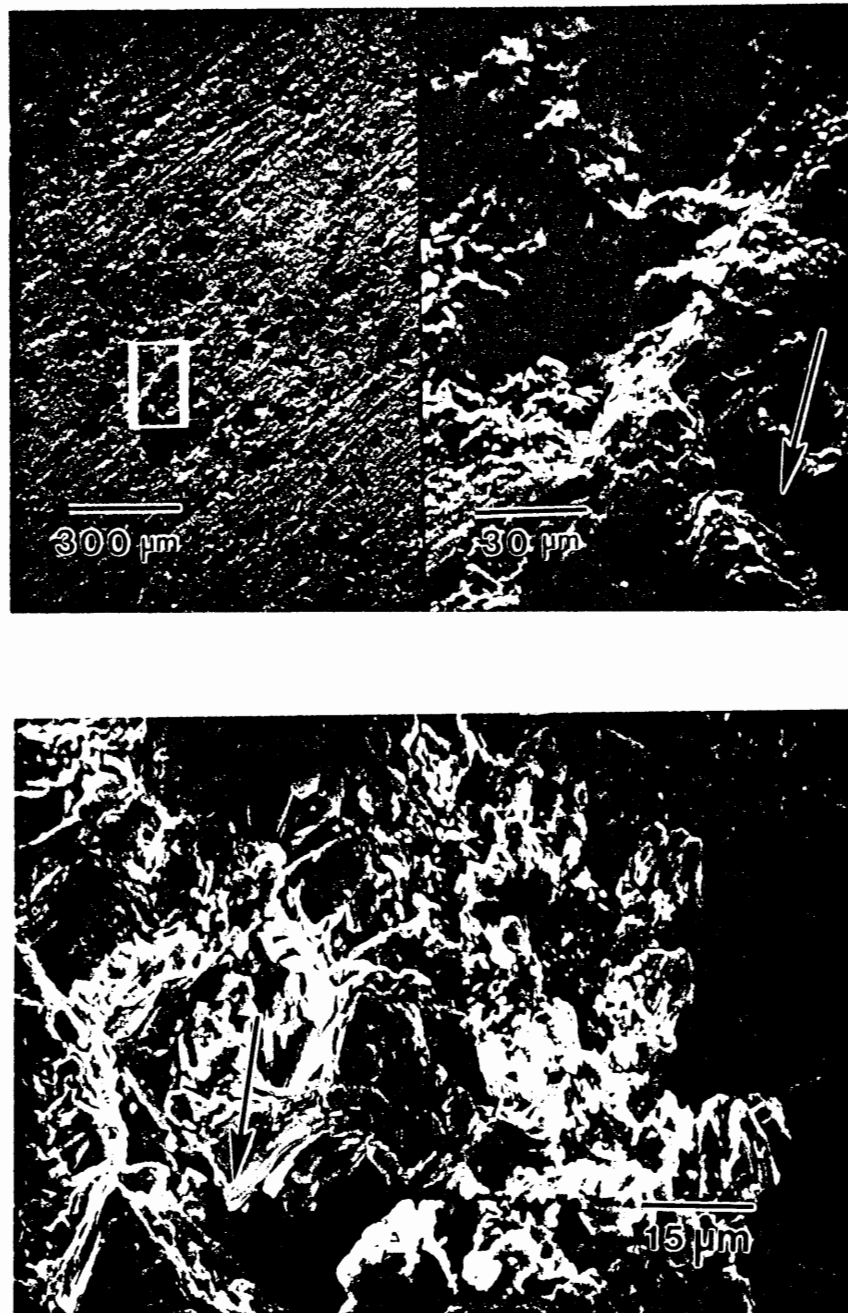


Figure 10. SEM micrographs of sample Bi #7 before exposure in the ballistic compressor. The surface shows a granular structure, the edges of the grains are sharp. Some particles are arranged regularly. The arrows mark corresponding features.

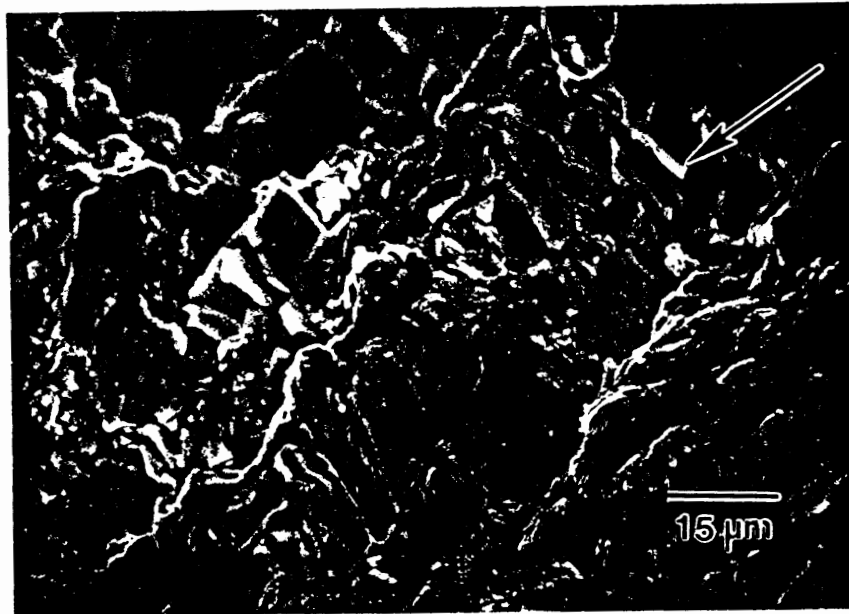
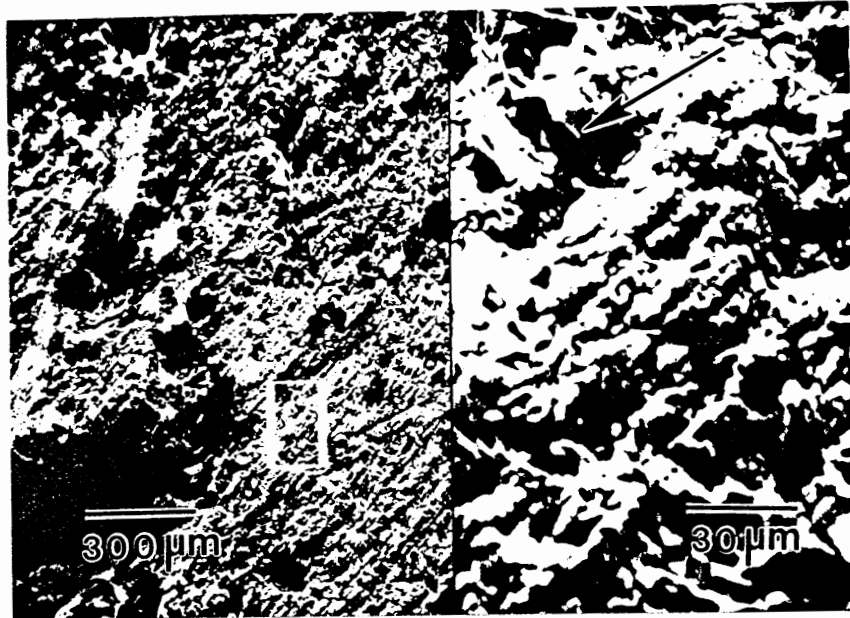


Figure 11. SEM micrographs of sample Bi #7 after double exposure in the ballistic compressor. The surface morphology seems almost unaffected. The edges of the grains look rounded due to heating. The arrows mark corresponding features.

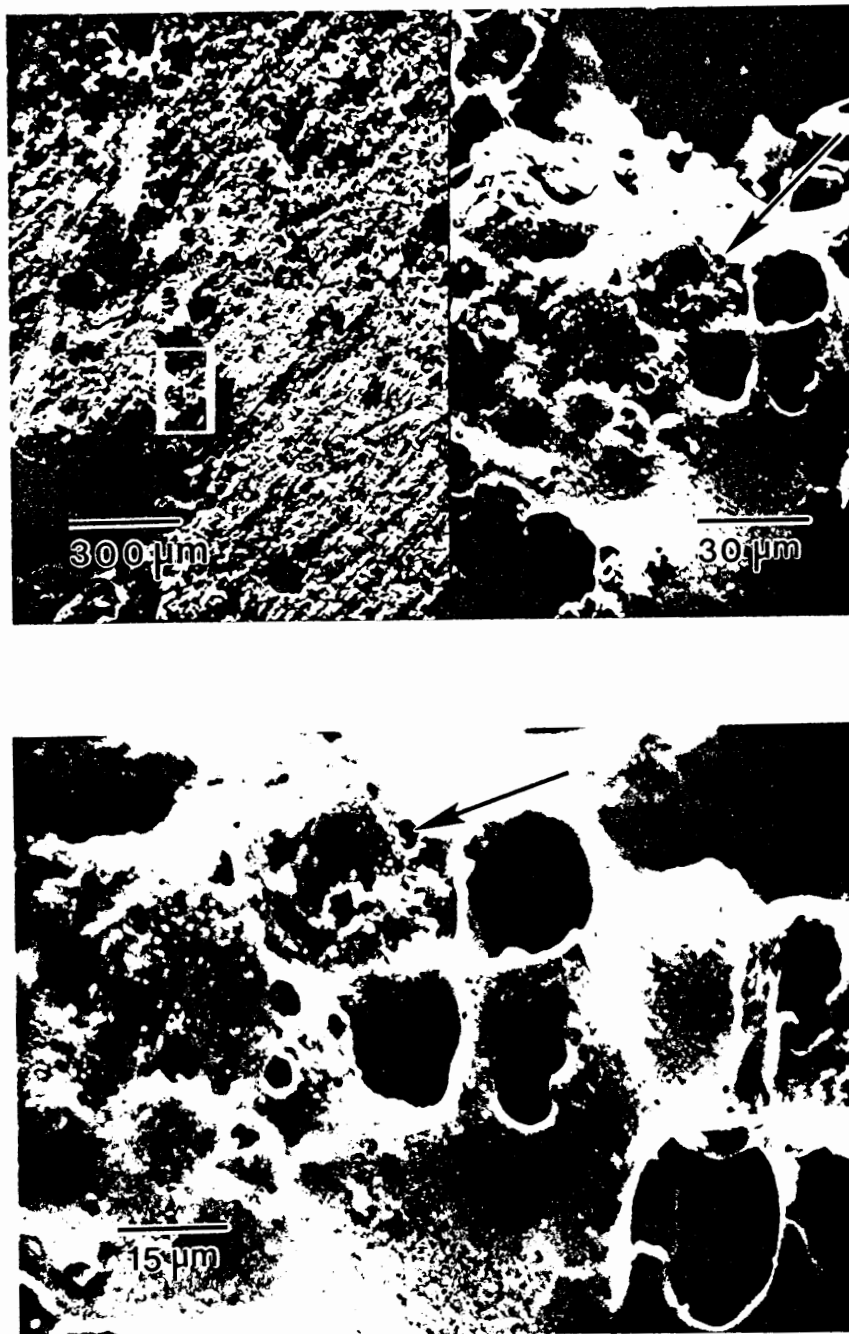


Figure 12. SEM micrographs of sample Bi #7 after double exposure in the ballistic compressor. This part of the surface is completely melted. The arrows in the images mark corresponding features.

Findings of Other Researchers

The morphology of unexposed samples was also investigated by other researchers.

Duan and Dash [17] investigated samples of a nominal composition $\text{Bi}_2\text{Sr}_2\text{CaCu}_2\text{O}_y$, which were prepared in a way similar to samples Bi #1 and #7. The particle size of the larger particles is similarly about $5 \mu\text{m}$. Although the compounds are different, the surface structure looks very similar.

Powers [26] displays an SEM image of "the porous microstructure of an as received BiCaSrCuO (*sic*) sintered pellet." The particle size compared to the one in Figures 8 and 10, is slightly larger, about $7 \mu\text{m}$. In addition, the amount of the fiber like particles is higher than that in Figures 8 and 10; the fiber length increased similarly to the particle size. Nevertheless, the structure shown in [26] looks similar to that in Figures 8 and 10, as well as [17].

Pissas, *et al.* [6] illustrate morphologies of Pb-doped nominal $\text{Bi}_{2-x}\text{Pb}_x\text{Sr}_2\text{Ca}_2\text{Cu}_3\text{O}_y$ compounds for x values between 0.1 and 0.5, which give the amount of added Pb. They observed a gradual increase of the size of the plate-like grains with increasing x from x = 0.1 to 0.4, and a certain degree of preferred orientation among the lamellar crystals.

EDS ANALYSIS

Qualitative Analysis

A qualitative analysis of the chemical surface composition of the samples was conducted in a SEM (ISI SS40) equipped with an EDS (Link). The electron energy was 25 keV.

The peak intensity ratios of the $Sr(L_{\alpha,\beta})$, $Bi(M_{\alpha,\beta})$, $Ca(K_{\alpha})$, and $Cu(K_{\alpha})$ peaks of all samples of nominal composition $Bi_{1.8}Pb_{0.2}Sr_2Ca_2Cu_3O_y$ investigated throughout this work, are given in Table V. Pb peaks were not observed.

TABLE V

INTENSITY RATIOS OF $Sr(L_{\alpha,\beta}) : Bi(M_{\alpha,\beta}) : Ca(K_{\alpha}) : Cu(K_{\alpha})$ PEAKS.
SPECTRA TAKEN FROM THE SURFACE OF SAMPLES WITH
NOMINAL COMPOSITION $Bi_{1.8}Pb_{0.2}Sr_2Ca_2Cu_3O_y$

Bi	no BC	1 x BC	2 x BC	3 x BC
#1	11:44:29:16	16:40:29:15	15:35:28:22	15:41:25:19
#2	11:39:29:21	16:39:26:19		
#3	13:42:29:16			
#4	11:39:27:23			
#7	13:41:27:19	14:38:27:21	16:40:27:17	
#8	13:45:25:17			
#10	13:45:24:18			

Figure 13 shows EDS spectra taken from sample Bi #7 before and after two exposures to hot, dense argon. To allow comparison between the different spectra they were always taken from the same area on the pellets; shown in Figure 14.

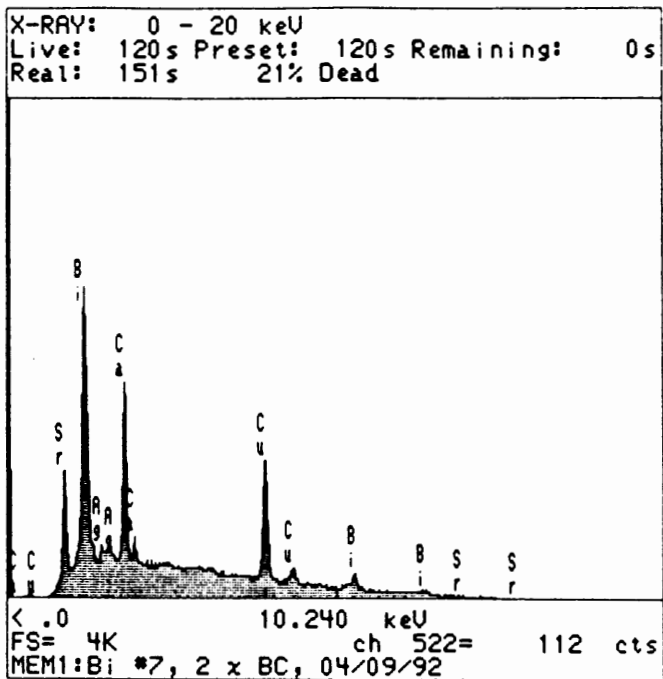
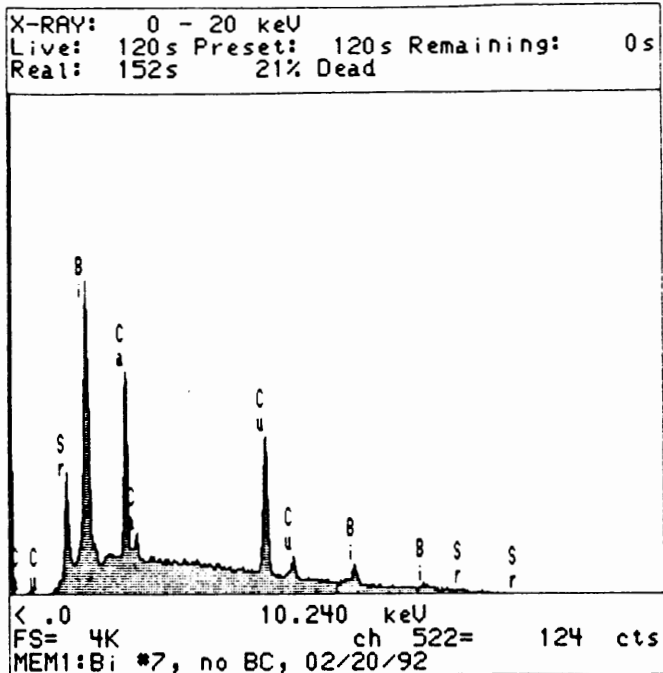


Figure 13. EDS spectra from sample Bi #7 before (upper) and after double exposure (lower) in the ballistic compressor. The spectra were taken from the area, shown in Figure 14, at an electron energy of 25 keV.

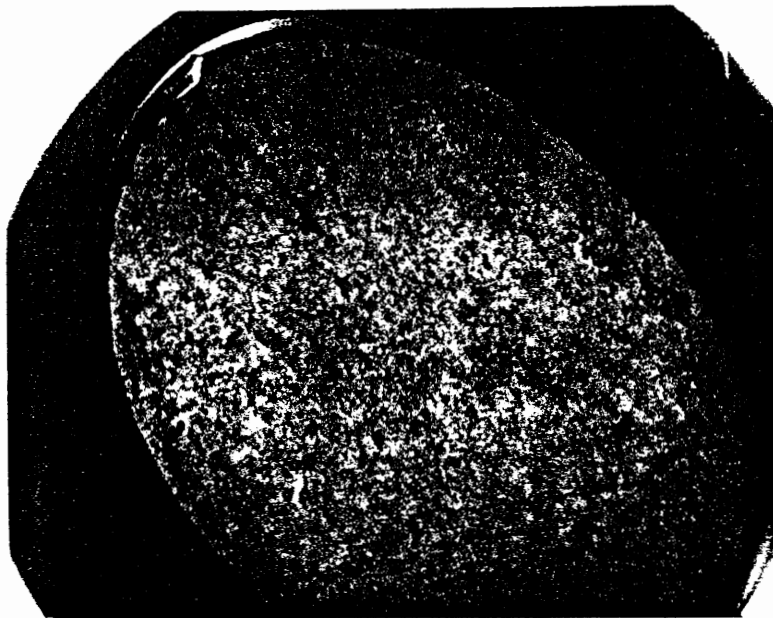


Figure 14. SEM micrograph of sample Bi #7. EDS spectra were always taken from the marked area.

Discussion

As seen from the results in Table V, the chemical surface composition of the samples varies greatly, considering an estimated 1% concentration being detectable [27] by the EDS.

Minimal and maximal values of observed relative peak height for each element before exposure in the ballistic compressor and the respective values for each element after exposure in the ballistic compressor are given in Table VI.

Comparison of the data shows that the relative peak height of the $Sr(L\alpha, \beta)$ peak increased after exposure of the samples in the ballistic compressor. This observation is met by all samples, as shown in Table V. A clear change in relative peak height was not observed for the other elements.

TABLE VI
 MAXIMAL AND MINIMAL VALUES OF OBSERVED RELATIVE
 PEAK HEIGHT FOR EACH ELEMENT, BEFORE AND
 AFTER EXPOSURE IN THE
 BALLISTIC COMPRESSOR

Element	Before Exposure	After Exposure
Sr	min. 11, max. 13	min. 14, max. 16
Bi	min. 39, max. 45	min. 35, max. 43
Ca	min. 24, max. 29	min. 23, max. 29
Cu	min. 16, max. 23	min. 15, max. 22

A clear statement about changes in the surface composition, due to exposure in the ballistic compressor, is not possible, concerning the elements Bi, Ca, and Cu. A clear increase or decrease of these elements is not consistently shown by all samples; see Table V.

The data indicate an increasing amount of Sr due to the thermal treatment in the ballistic compressor.

The presence of Ag in the spectrum of sample Bi #7 after double exposure in the ballistic compressor can be explained by remainders of silver paint which were not removed completely from the sample surface.

There are two reasons for the absence of Pb peaks in the spectra. The first reason is that the Pb peaks are closely located to the Bi peaks; the Pb($M\alpha$) and the Bi($M\alpha$) lines have energies of 2.342 keV and 2.418 keV, respectively [28]. Thus it is possible that the Bi peaks contain tiny Pb peaks, which are not resolved on this scale. The second possibility is

evaporation of Pb during the annealing process. A partial loss of Pb during heat treatment was observed before by Jasiolek, *et al.* [7] and Vassilev, *et al.* [29].

Figure 15 shows the surface structure of sample Bi #4 before exposure to hot, dense argon in the ballistic compressor, which is typical for $\text{Bi}_{1.8}\text{Pb}_{0.2}\text{Sr}_2\text{Ca}_2\text{Cu}_3\text{O}_y$ superconductor pellets before the rapid heating and cooling process.

The particle size of the larger "cornflake"-like particles is about 5 μm . Fiber-like particles, which are about 5 μm long are also found.

Two EDS spectra were taken from a typical fiber-like particle (arrow 1 and 2) and one from a typical "cornflake"-like particle (arrow C).

The results of the qualitative EDS analysis are shown in Table VII. The two spectra taken from the fiber-like particle are shown in Figure 16, the spectrum from the "cornflake"-like particle is shown in Figure 17.

TABLE VII

INTENSITY RATIOS OF $\text{Sr}(L\alpha, \beta) : \text{Bi}(M\alpha, \beta) : \text{Ca}(K\alpha) : \text{Cu}(K\alpha)$ PEAKS. SPECTRA TAKEN FROM THE SURFACE OF SAMPLE Bi #4 BEFORE EXPOSURE IN THE BALLISTIC COMPRESSOR. (C) "CORNFLAKE"-LIKE PARTICLE; (1) AND (2) FIBER-LIKE PARTICLE

Sample	(C)	(1)	(2)
Bi #4	15:49:20:16	12:45:20:23	13:45:19:23

Comparison of the two EDS spectra taken from two different points of the same fiber-like particle demonstrate homogeneity. The EDS data taken from the "cornflake"-like particle show a lower amount of Cu and an increased amount of Bi and Sr, compared to the fiber-like particle.

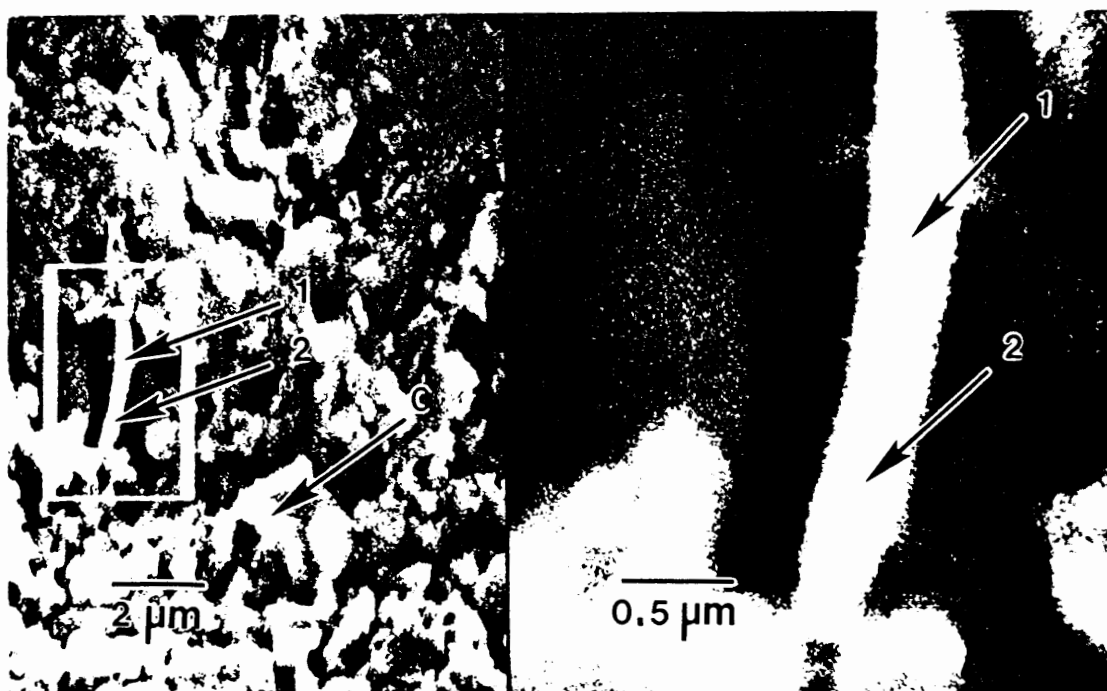


Figure 15. SEM micrograph of the surface structure of sample Bi #4 before exposure in the ballistic compressor. (C) marks a typical "corn-flake"-like particle, (1) and (2) mark a typical fiber-like particle.

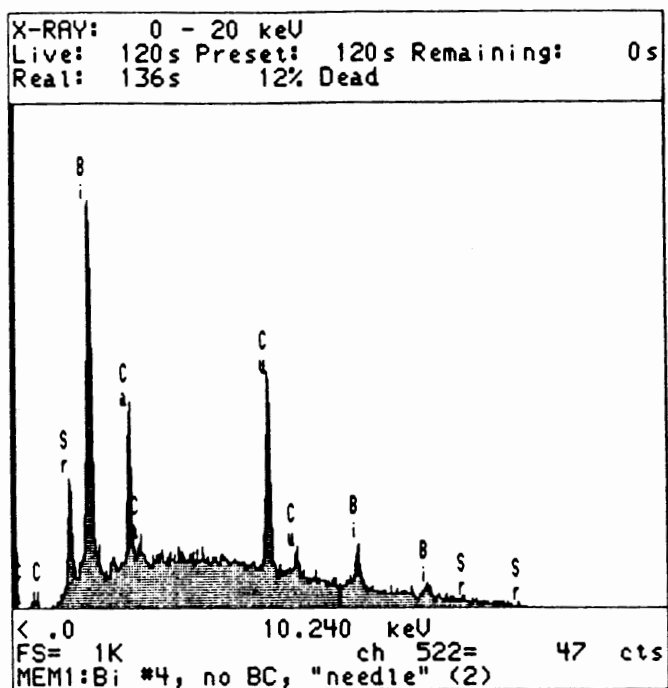
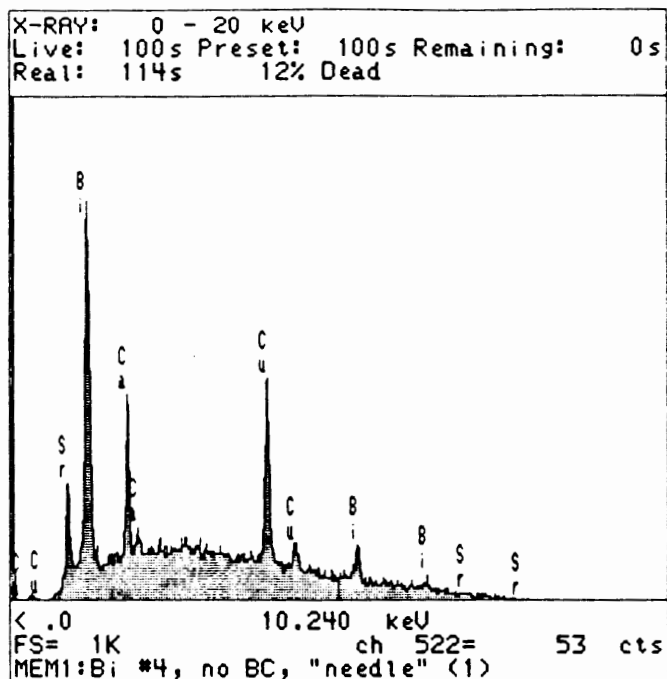


Figure 16. EDS spectra of the fiber-like particles, marked in Figure 15 by arrow (1) (upper) and arrow (2) (lower). The energy of the electrons was 25 keV.

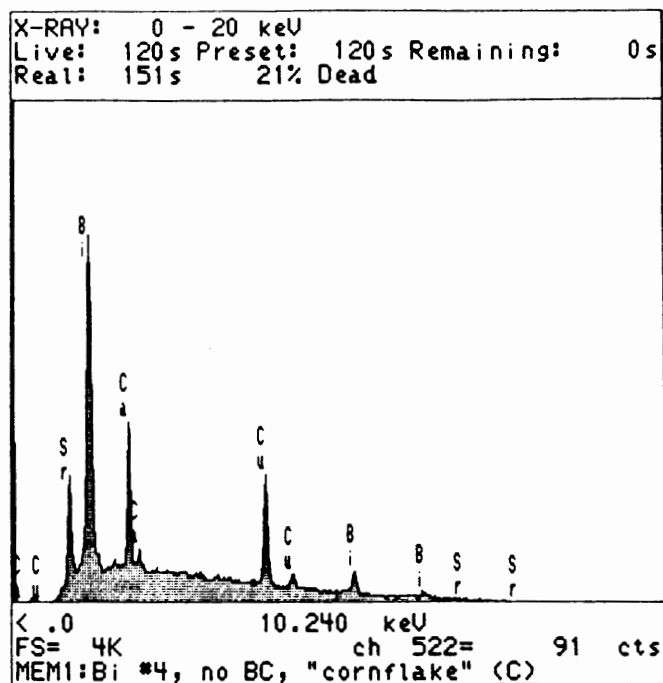


Figure 17. EDS spectrum of the "cornflake"-like particle, marked in Figure 15 by arrow (C). The electron energy was 25 keV.

Findings of Other Researchers

The large variations in chemical composition of the Bi compounds were observed before. Jasiolek, *et al.* [7] "used microprobe (EPMA) techniques for the characterization of the high-temperature superconducting materials". They found that "the compositions of the superconducting grains or crystals tested by the EPMA technique gave varying results" [7].

Qualitative Analysis of Oxygen Content

Motivation for further EDS investigations was owing to Nagoshi, *et al.* [30], who reported an increase in the critical

temperature after a vacuum annealing process, which caused a small amount of oxygen loss, and to Peuckert, *et al.* [31], who found a decreasing transition temperature after a special thermal procedure, with increasing amount of oxygen.

Duan, *et al.* [17,18] reported an increase in critical temperature after exposure of samples to hot, dense argon. The effect of the exposure in the ballistic compressor on the oxygen content in the sample surface is subject to current investigations [32].

In the present investigation, a qualitative EDS analysis was conducted on both sides of samples Bi #1 and #7 as well as on the cross-sectional area of both pellets. The use of a thin window instead of the 7.5 μm Be window enabled the detection of elements with atomic numbers lower than 11. Each spectrum was taken at two different accelerating voltages of the SEM; 10 kV and 20 kV, respectively. The peak intensity ratios of the O($K\alpha$) and Cu($L\alpha,\beta$) peaks observed at different areas and different accelerating voltage are given in Table VIII. EDS spectra of sample Bi #1, taken in the cross-section at 10 kV, are shown in Figure 18.

Discussion of Oxygen Investigation

The data given in Table VIII do not show clearly, whether the O($K\alpha$) : Cu($L\alpha,\beta$) ratio is affected by exposure to hot, dense argon, or not. Comparison of spectra taken on both the unexposed and on the exposed side indicate a slight increase

TABLE VIII

INTENSITY RATIOS OF $O(K\alpha):Cu(L\alpha,\beta)$ PEAKS. SPECTRA WERE TAKEN FROM BOTH SAMPLE SURFACES, (a) UNEXPOSED SIDE, (b) EXPOSED SIDE AND FROM TWO REGIONS IN THE CROSS-SECTION OF THE PELLET, (c) CLOSE TO THE UNEXPOSED SIDE AND (d) CLOSE TO THE EXPOSED SIDE

Sample #	(a)	(b)	(c)	(d)
Bi #1, 10 KV	84:16	87:13	80:20	76:24
20 KV	83:17	91:09	79:21	69:31
Bi #7, 10 KV	82:18	85:15		
20 KV	79:21	79:21	72:28	67:33

in the $O(K\alpha):Cu(L\alpha,\beta)$ ratio. Spectra from the cross-sections of both samples show a slight decrease. They were taken from a square area of approximately $400 \mu\text{m}^2$, one time close to the unexposed side and another time close to the exposed side,

The penetration depth of the electrons is less than $1 \mu\text{m}$ [27] for both, 10 kV and 20 kV, accelerating voltage, which is far less than the thickness of the affected surface layer. Hence, different results at different accelerating voltages demonstrate the inhomogeneity of the samples.

However, the results do not oppose the reported changes in oxygen content by [30,31], which were on the order of 10^{-3} [30] and not detectable with the EDS used in this work.

The hoped-for larger oxygen decrease due to exposure of the pellets in the ballistic compressor could not be demonstrated.

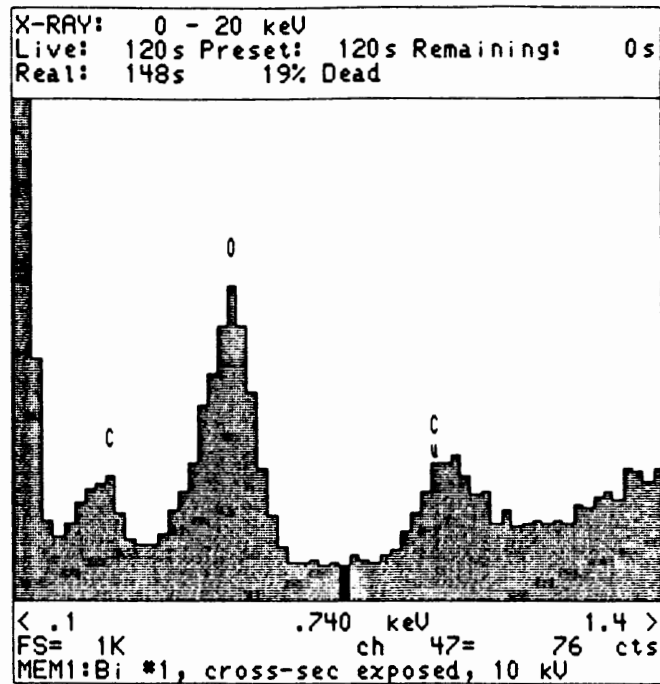
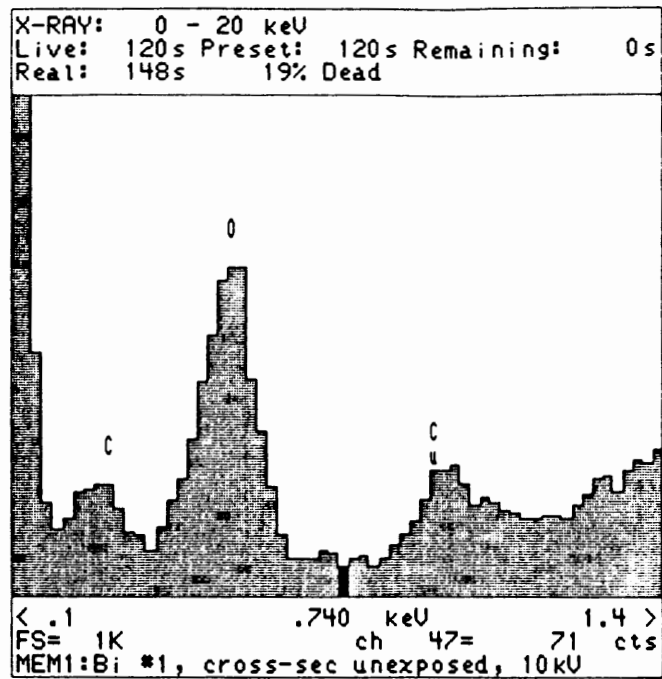


Figure 18. EDS spectra of sample Bi #1 of the cross-sectional area. Both spectra were taken of an area of $400 \mu\text{m}^2$ one time close to the unexposed side (upper) and one time close to the exposed side (lower). The electron energy was 10 keV.

X-RAY DIFFRACTION STUDIES

X-ray diffraction analysis was conducted with a Philips XRG-3000 diffractometer, which uses $\text{Cu}(K\alpha)$ radiation with a radiation wavelength $\lambda=1.54178 \text{ \AA}$. The positions of the peaks were read from a diffractograph, which was scanned at a speed of $1^\circ/\text{minute}$; the chart speed was $0.5 \text{ inch}/^\circ$.

Specimens Bi #1 and #7 were investigated before and after each of the subsequent exposures in the ballistic compressor. The purpose of the x-ray diffraction studies was to determine if exposure to hot, dense argon causes any change in the relative amount of the $n = 1$, $n = 2$ or $n = 3$ phase.

Indexing

The peak positions on the diffractograph give the d-spacings of the respective crystal planes, which are evaluated by means of Bragg's Law,

$$2d_m \sin \theta = n\lambda$$

where d_m is the d-spacing of the crystal plane, evaluated from the measured peak position, λ is the radiation wavelength (here $\text{Cu}(K\alpha)$ radiation with $\lambda=1.54178 \text{ \AA}$), and θ is the glancing angle of incidence, n is an integer with $n > 0$. By convention all angles are given in the following in terms of 2θ . Since the lattice parameters of the three different superconducting phases, present in the multiphase compound, are known [5,9], one can evaluate d-spacings for most of the

possible crystal planes theoretically present in the mixture of the three phases, assuming that there is no change of the lattice parameters due to exposure of the samples in the ballistic compressor. For tetragonal structures, the distance d is given by [33],

$$\frac{1}{d_c^2} = \frac{h^2 + k^2}{a^2} + \frac{l^2}{c^2}$$

where d_c are the calculated d-spacings, and the (hkl) are the Miller indices of the respective plane. Lattice parameters for the three superconducting phases were given before in Table I; $a = b = 5.4 \text{ \AA}$, the c lattice parameter increases from 24.4 to 30.76 and then to 37.1 \AA [5,9], in going from the $n = 1$ to the $n = 2$ and $n = 3$ phase.

Comparison of the theoretically evaluated d-spacings (d_c) with the experimentally determined ones (d_m), reveals the (hkl) and the phase of the reflecting plane.

For this purpose, a computer program was written, which evaluated d-spacings from the $(h=0 \ k=0 \ l=1)$ plane, up to the $(h=14 \ k=14 \ l=24)$ plane for the $n = 1$, $n = 2$, and $n = 3$ phase, respectively. Each d-spacing, connected to a peak in the spectrum was compared with the 14112 values calculated by the computer program.

Indexing of the peaks in the diffractographs and determination of the relative peak heights was not easy,

because a lot of peaks overlap. The investigated specimens consist of three phases with tetragonal structure; the lattice parameters in a and b direction are equal ($a = b = 5.4 \text{ \AA}$). Hence, a lot of overlaps in the (hk0) planes are expected.

Since the space groups of the structure are unknown, systematic extinctions of the peaks could not be taken into account. This would have helped in indexing the peaks in the diffractographs. Assignment of several peaks to a certain plane and phase was not clearly possible due to peak overlaps.

The background in the diffractographs was approximated by drawing a line from the background at lower angles ($2\theta = 8^\circ$ to 12°) to the background at angles of $2\theta = 60^\circ$ to 62° . This approximated background was subtracted from the measured height of the peaks. Subsequently, the intensity of each peak was divided by the intensity of the highest peak in the respective spectrum. However, the background and the peak overlap admitted only a crude estimate for peaks with low intensities. Peaks with relative intensities lower than 20 were inconclusive and left out in further considerations.

The result of this procedure is shown in Tables IX and X. Given are the (hkl), the angle 2θ , the relative peak height I/I_0 before and after exposure of the samples in the ballistic compressor, the calculated d-spacing d_c in (\AA), the d-spacing d_m , evaluated from the measured peak positions in (\AA), and the phase n ($n = 1, 2, \text{ or } 3$), for peaks up to 60° .

Discussion

The presence of the three phases was confirmed in both samples Bi #1 and Bi #7.

In the diffractographs of sample Bi #1, 32 peaks between 2° and 60° showed a relative intensity which was higher than 20. Worth mentioning is a decrease in the absolute intensity of the peaks in the diffractograph after triple exposure to hot, dense argon by a factor of four. This phenomenon was accompanied by an increase of the general background by a factor of two. The decrease in absolute peak height is an indication for small crystals present in the surface.

The surface of sample Bi #1 was completely melted after triple exposure in the ballistic compressor. The high cooling rate in the firing process might have handicapped the melted material from recrystallization which yields smaller crystals in the surface. Observed line broadening indicates the formation of a surface layer with small crystals on sample Bi #1 due to the thermal treatment in the ballistic compressor.

Similar line broadening and a similar rise of the background after exposure of iron in the ballistic compressor was observed by Dash, *et al.* [15]. Argon seemed to diffuse into the material to expand the crystal, but details were not clear [15].

Comparing the data of sample Bi #1 before and after triple exposure in the ballistic compressor, yields a general increase in relative intensity of all peaks (except three

peaks which decreased) after triple exposure in the ballistic compressor, independent of the phase.

If the amount of one particular phase would have increased, one would expect that the amount of at least one of the remaining phases decreased, assuming random crystal growth. This decrease in the amount of one of the three phases was not observed.

However, before exposure of sample Bi #1 in the ballistic compressor the strongest peak was reflected from a plane of the $n = 1$ phase, but after triple exposure in the ballistic compressor the strongest peak in the spectrum was reflected from a plane of the $n = 3$ phase. The "shoulder" peak at $2\theta = 27.5^\circ$ which was resolved only after triple exposure in the ballistic compressor was reflected from a lattice plane of the $n = 3$ phase; see Table IX.

The general increase in the relative peak intensity was ascribed to the random crystal growth after triple exposure in the ballistic compressor.

In the diffractographs of sample Bi #7, 26 peaks between 2° and 60° showed a relative intensity which was higher than 20. The absolute intensity of the peaks after double exposure in the ballistic compressor did not change significantly.

A consistent change of the relative peak heights could not be demonstrated. Three new peaks are listed in Table X after double exposure in the ballistic compressor. All three peaks are "shoulder" peaks which were not resolved in the

diffractograph before exposure in the ballistic compressor. Two of these peaks were reflected from planes of the $n = 3$ phase, one was reflected from a plane of the $n = 2$ phase.

Crystallite Size

Measurements of the half-maximum line width (W), which is connected to the crystal sizes of the particles, should give information about differences appearing due to exposure in the ballistic compressor.

The basis for the measurement of crystallite size by this method is the observation that the diffracted beam becomes diffuse, when the crystal size gets close to the wavelength of the incident beam [34]. The relationship between crystallite size and x-ray line broadening was first derived by P. Scherrer [34]. He showed, that the line broadening is due to crystallite size effects as well as an instrumental broadening of the lines [34,35].

Other factors which yield line broadening of the peaks in the x-ray diffractographs are the distortion of the crystal structure and local differences in the thermal expansion of the lattice which might be caused by exposure of the material to hot, dense argon in the ballistic compressor. Distortions of the crystal lattice are known to be present in the investigated material. Thermal expansions of the lattice are very likely to occur due to exposure of the samples in the ballistic compressor. Hence, the subsequent evaluations of the crystal size are more a rough estimate.

TABLE IX

X-RAY DIFFRACTION DATA FOR SAMPLE Bi #1 BEFORE AND AFTER
TRIPLE EXPOSURE IN THE BALLISTIC COMPRESSOR

2 θ	d_c	(hkl)	before exp.				after exp.			
			I/I ₀	d_m n=1	d_m n=2	d_m n=3	I/I ₀	d_m n=1	d_m n=2	d_m n=3
23.3	3.82	1 1 0	46.5			3.82	40.0			3.83
25.2	3.53	1 1 4	32.0			3.55	25.0			3.56
25.3	3.52	0 1 8	8.0			3.51	28.5			3.51
27.5	3.25	1 1 6) ¹				70.0			3.26
27.6	3.24	1 1 4	100	3.23			88.5	3.23		
28.5	3.13	0 1 8	12.5		3.14		48.5		3.14	
29.2	3.06	1 1 6	52.0		3.07		85.0		3.07	
29.7	3.01	1 1 5	18.0	3.02			43.5	3.01		
30.3	2.95	1 1 8	19.0			2.98	51.5			2.97
31.3	2.86	0 1 11	92.0			2.87	100			2.86
32.0	2.80	1 1 9	10.0			2.81	38.5			2.81
33.3	2.69	0 2 1	78.0		2.69		70.0		2.68	
33.8	2.65	0 0 14	12.5			2.65	25.0			2.65
35.0	2.56	0 0 12	42.0) ²		2.56		50.0) ²		2.56	
35.0	2.56	0 2 3		2.56				2.56		
35.4	2.54	0 2 5	46.5			2.54	55.0			2.54

TABLE IX

X-RAY DIFFRACTION DATA FOR SAMPLE Bi #1 BEFORE AND AFTER
TRIPLE EXPOSURE IN THE BALLISTIC COMPRESSOR
(continued)

35.6	2.52	1 0 13	26.5			2.52	58.5			2.51
36.4	2.47	0 2 4	18.0	2.46			50.0	2.46		
38.3	2.35	1 2 3	6.5		2.35		65.0		2.35	
38.9	2.32	1 2 3	25.5	2.32			56.5	2.31		
43.4	2.08	1 2 9	7.5			2.09	35.0			2.09
44.8	2.02	0 1 17	56.5			2.02	78.5			2.03
45.0	2.01	1 1 13	27.5		2.01		33.5		2.01	
46.5	1.95	0 0 19	6.5			1.95	30.0			1.95
47.3	1.92	0 0 16	13.5		1.92		26.5		1.92	
47.6	1.91	2 2 0	43.5			1.91	51.5			1.90
49.1	1.86	0 0 20	22.5			1.86	38.5			1.86
50.6	1.80	2 1 9	41.0	1.80			53.5	1.81		
53.7	1.71	1 3 0	16.5) ³			1.71	33.5) ³			1.70
53.7	1.71	1 3 1								
54.9	1.67	1 3 3	10.0	1.67			30.0	1.67		
56.1	1.64	2 0 18	29.0			1.64	38.5			1.64
56.9	1.62	2 2 8	16.5	1.62			36.5	1.62		

TABLE IX

X-RAY DIFFRACTION DATA FOR SAMPLE Bi #1 BEFORE AND AFTER
 TRIPLE EXPOSURE IN THE BALLISTIC COMPRESSOR
 (continued)

58.1	1.59	3 0 11	23.5) ³			1.59	28.5) ³			1.59
58.1	1.59	2 2 13								

-)¹ "Shoulder" peak which was not resolved in the diffractograph before exposure of the sample in the ballistic compressor.
-)² The peak can be ascribed to two or more different planes of different phases.
-)³ The peak can be ascribed to two different planes of the same phase.

TABLE X

X-RAY DIFFRACTION DATA FOR SAMPLE Bi #7 BEFORE AND AFTER
DOUBLE EXPOSURE IN THE BALLISTIC COMPRESSOR

2θ	d _c	(hkl)	before exp.				after exp.			
			I/I ₀	d _m n=1	d _m n=2	d _m n=3	I/I ₀	d _m n=1	d _m n=2	d _m n=3
23.1	3.85	0 0 8	86.5		3.87		76.0		3.87	
24.6	3.62	0 1 5	26.0) ¹	3.60						
24.9	3.58	1 1 3						26.5) ¹		3.58
27.2	3.28	1 0 9	95.0			3.27	93.0			3.26
28.8	3.10	1 1 7	100			3.10	100			3.09
31.0	2.89	0 1 9	91.0		2.90		84.0		2.89	
31.3	2.85	0 0 13	24.5			2.82	18.0			2.85
32.0	2.80	1 1 9	19.5			2.81	32.5			2.81
32.2	2.78	1 1 6	9.0	2.77			25.0	2.79		
33.0	2.71	0 0 9	55.5	2.71			45.5	2.71		
33.2	2.70	0 2 0) ²				45.5			2.70
33.5	2.67	1 0 10	23.0		2.68					
33.5	2.67	0 2 2) ¹) ³			2.68				
33.7	2.66	1 1 10					20.0) ¹			2.66
34.9	2.57	1 1 7	99.5	2.58			69.5	2.57		

TABLE X

X-RAY DIFFRACTION DATA FOR SAMPLE Bi #7 BEFORE AND AFTER
DOUBLE EXPOSURE IN THE BALLISTIC COMPRESSOR
(continued)

35.2	2.55	0 2 4) ²				49.5) ⁴		2.55	
35.2	2.55	1 1 9								
36.3	2.47	0 2 6	13.5) ⁴			2.48	24.0) ⁴		2.48	
36.3	2.47	0 0 15								
44.5	2.04	0 1 14	61.0		2.04		55.5		2.03	
44.8	2.02	1 2 10	36.5) ⁴			2.03	29.5) ⁴		2.02	
44.8	2.02	0 1 17								
47.2	1.93	1 0 18	26.0			1.93	26.5		1.93	
47.5	1.91	0 2 9	42.0) ³	1.91			39.5) ³	1.91		
47.6	1.91	2 2 0								1.91
47.8	1.90	1 0 12	21.3	1.90) ⁵			
48.7	1.87	2 2 4	27.0) ¹			1.87				
49.0	1.86	0 2 12					25.0) ¹		1.86	
50.3	1.81	1 1 18	62.0			1.81	54.5		1.81	
55.7	1.65	3 0 9) ²				21.0			1.65
56.1	1.64	2 0 18	36.0			1.64	35.5		1.64	
56.6	1.63	0 0 15	19.5) ³	1.63			22.0) ³	1.62		

TABLE X

X-RAY DIFFRACTION DATA FOR SAMPLE Bi #7 BEFORE AND AFTER
DOUBLE EXPOSURE IN THE BALLISTIC COMPRESSOR
(continued)

56.6	1.63	1 3 7) ³			1.63) ³			1.62
56.6	1.63	1 2 14			1.63				1.62	
57.9	1.59	0 3 9	21.5		1.60		19.0		1.59	
59.8	1.55	1 0 23	35.5			1.54	26.5			1.54

-)¹ The reflecting plane could not be determined. The peaks before and after exposure in the ballistic compressor are ascribed to two different planes, although they are corresponding peaks.
-)² "Shoulder" peak which was not resolved in the diffractograph before exposure of the sample in the ballistic compressor.
-)³ The peak can be ascribed to two or more different planes of different phases.
-)⁴ The peak can be ascribed to two different planes of the same phase.
-)⁵ "Shoulder" peak which was not resolved in the diffractograph after exposure of the sample in the ballistic compressor.

Since in most cases the crystallite shape is unknown and may vary between crystals, Bragg [35] defined D as the mean dimension of the crystallite perpendicular to the diffraction planes. From this assumption, he derived the simplified equation,

$$D = \frac{51\lambda}{W\cos\theta}$$

where the average crystallite dimension D is directly proportional to the radiation wavelength λ in Å, W is the half-maximum width of the line in degrees, and θ is the incidence angle.

This allows us to dispense with corrections due to instrumental broadening [34], if we are interested in an estimation of the size of the crystal particles [35].

The six peaks with the highest relative intensity in the spectrum taken before exposure in the ballistic compressor are compared to the corresponding peaks in the spectrum after exposure in the ballistic compressor.

Tables XI and XII show the crystal size of sample Bi #1 before and after exposure in the ballistic compressor, respectively. Tables XIII and XIV show the respective data of sample Bi #7.

The crystal size in sample Bi #1 decreased with exposure in the ballistic compressor, as seen from Tables XII and XIII. The high cooling rate seems to handicap the melted material

from recrystallization which yields smaller crystals. The observation of the general increase in relative peak height in the spectrum of sample Bi #1 after triple exposure in the ballistic compressor and the line broadening indicate the formation of small crystals in the surface layer.

TABLE XI

CRYSTAL SIZES IN SAMPLE Bi #1 BEFORE EXPOSURE
IN THE BALLISTIC COMPRESSOR

2θ	I/I_0	$W [^\circ]$	$D [\text{\AA}]$
27.6	100	0.32	253
31.3	92.0	0.32	255
33.3	78.0	0.32	257
44.8	56.5	0.55	155
29.2	52.0	0.32	254
23.3	46.5	0.32	251

TABLE XII

CRYSTAL SIZES IN SAMPLE Bi #1 AFTER THIRD EXPOSURE
IN THE BALLISTIC COMPRESSOR

2θ	I/I_0	$W [^\circ]$	$D [\text{\AA}]$
27.6	88.5	0.39	208
31.3	100	0.43	190
33.3	70.0	0.32	257
44.8	78.5	0.63	135
29.2	85.0	0.47	173
23.3	40.0	0.35	229

TABLE XIII

CRYSTAL SIZES IN SAMPLE Bi #7 BEFORE EXPOSURE
IN THE BALLISTIC COMPRESSOR

2θ	I/I_0	$W [^\circ]$	$D [\text{\AA}]$
28.8	100	0.32	254
34.9	99.5	0.47	175
27.2	95.0	0.32	253
31.0	91.0	0.35	233
23.1	86.5	0.32	251
50.3	62.0	0.32	271

TABLE XIV

CRYSTAL SIZES IN SAMPLE Bi #7 AFTER SECOND EXPOSURE
IN THE BALLISTIC COMPRESSOR

2θ	I/I_0	$W [^\circ]$	$D [\text{\AA}]$
28.8	100	0.24	338
34.9	69.5	0.39	211
27.2	93.0	0.24	337
31.0	84.0	0.24	340
23.1	76.0	0.24	334
50.3	54.5	0.28	310

Contrarily, the crystal size increased in sample Bi #7. This result is unexpected, however, it is in accordance with Duan [23], who also observed both line broadening and narrowing after exposure of samples in the ballistic compressor.

T_c MEASUREMENTS

Superconductors have besides the normal conducting phase a superconducting phase, which appears below a critical temperature T_c . The superconducting state is characterized by the Meissner effect, which was described before, and a vanishing electrical resistance.

Since an experiment can only give an upper limit for the resistance, it is impossible to measure that the resistance is really zero. However, the resistance of superconductors was determined to be at least 10^{17} orders of magnitude less, than that of copper [33], which is practically seen, as "zero-resistance".

Experiment

Measurements of the transition temperature were taken in a standard four-point probe configuration, shown in Figure 19. Electrical contacts on the pellets were made by using silver paint. The lead wires were tinned copper wires (#28) with a diameter of 0.32 mm and a resistance of 0.2129 ohms per meter at 20 °C. The temperature of the specimens was measured by means of a copper constantan thermocouple, which was taped on the surface of the specimens. Heat conduction through the lead wires and the thermocouple wire was assumed to be small. After exposure of the samples in the ballistic compressor, the positions for contacts and thermocouple were found again by means of a marker which was scratched in the surface of the

pellets. A constant current between $I = 15 \text{ mA}$ to $I = 30 \text{ mA}$ was applied to the contacts 1 and 4; see Figure 19. The voltage between contacts 2 and 3, which is primarily a function of the resistance between the both contacts, was plotted constantly along with the temperature on the pellet surface. The input impedance of the chart writer was 20 MegOhms through 100 mV, the sensitivity was 0.05 mV.

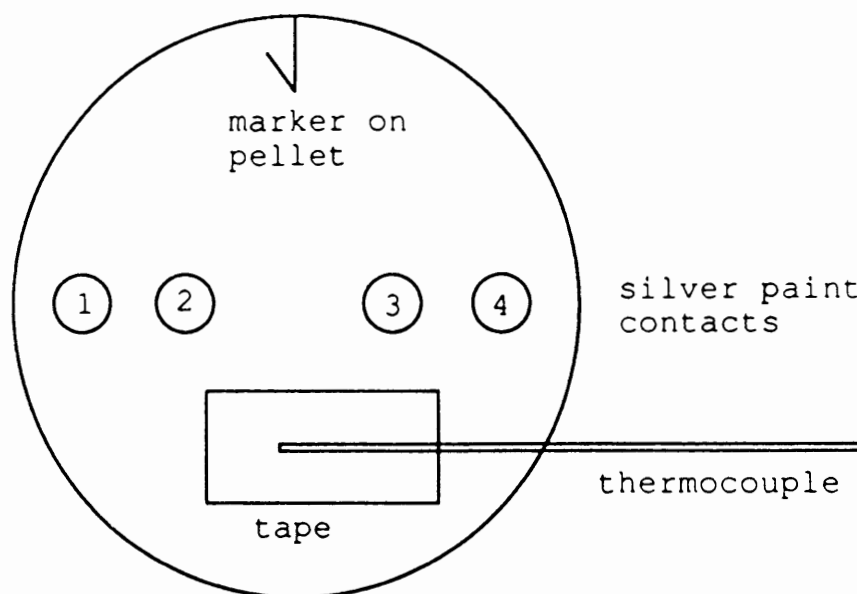


Figure 19. Standard four-point probe configuration. A constant current is applied to contacts 1 and 4. The voltage is measured between contacts 2 and 3.

All measurements were conducted in the "warming up" process. First, the specimens, which were placed in a styrofoam cup, were cooled down to liquid nitrogen temperature. As a result, the voltage between contacts 2 and 3 dropped down to "zero-voltage". Subsequently the liquid

nitrogen either evaporated or was quickly poured out of the styrofoam cup. Thereafter, the samples warmed up at a rate of 10 - 20 K per minute. At the critical temperature T_c , the voltage started rising, due to rising electrical resistance. The temperature, at which the voltage rise begins, is defined as the critical temperature of the superconductor. After travelling through the transition range, the resistance rise flattens at the "onset"; the superconductor is in the normal conducting phase. Subsequently the superconductor shows the resistivity characteristics of a metal, i.e. the resistance increases slowly with increasing temperature.

A two-step superconducting transition was reported by others after annealing samples at high temperatures. Hence, the shape of the curves obtained in these measurements was also a subject of interest, besides the determination of the transition temperature.

Results

The measured T_c values varied greatly, and their reproducibility remains a problem. It was observed that the obtained data throughout one experimental run were considerably constant. In the course of one experimental run the lead wires remained connected to the sample, while repeated cooling down and heating up cycles were performed. A new experimental run started after each dis- and reconnection of the lead wires to the sample. Very large variations were

observed when remeasuring the samples on another day. It was important to measure always in the same direction of the pellets. Measurements in directions perpendicular to each other yielded a different result. This was also observed by Duan, *et al.* [17]. It was observed earlier that T_c depends on the applied maximum voltage and on the applied constant current. In order to observe this effect, measurements were conducted on sample Bi #7, after one exposure in the ballistic compressor, at different voltages and currents, but with the same experimental setup; see Table XVI. Because of the uncertainty in the results obtained by the four-point probe method, several experiments were performed, special attention being paid on samples Bi #1 and #7. The results of the measured data are shown in Table XV. Each box of the table shows the data of one experimental run. Underlined numbers indicate that the thermocouple was stuck in a hole, which was drilled in the edge of the pellet. This method was used in the beginning, but changed later to the taping method, because it could not be guaranteed that the thermocouple touches every time the same position in the hole. A temperature gradient between top and bottom of the specimens was determined to be 7 to 15 K. Variations in the critical temperature of 3.5 to 7.5 K, depending on whether the thermocouple touched the "bottom" or the "upper part" of the hole would have been possible. Bold numbers represent measurements on the unexposed side of the samples.

TABLE XV

DATA OF T_c MEASUREMENTS BEFORE AND
AFTER EXPOSURE OF THE SAMPLES IN
THE BALLISTIC COMPRESSOR (BC)

Sample	No BC	1 x BC	2 x BC	3 x BC
Bi #1	<u>85/84/85</u>			<u>85/86/85</u>
				92/91/92 93/92
				92/92/93 93
				<u>88/87/86</u> <u>87/87</u>
				90/91/92 93/92
				<u>82/81/82</u> <u>82/81</u>
Bi #2	84/87/84/84			
Bi #3	87/86/84/87			
Bi #4	89/89/89			
Bi #5	98/100/100			
Bi #6	108/108/108			
Bi #7	99/99/100	124/122/122 125/121/123 122/124/128	100/100/101 101	
	99/101/99 99	116/118/118 117/116/121 118/123/114	104/105/103 104/104	
			99/100/97 97/99/97	
			99/99/99/99	
Bi #8	104/103/104			
	104/105/104			
	105/105/105			
Bi #9	101/100/100			
	82/82/85/85			

TABLE XV

DATA OF T_c MEASUREMENTS BEFORE AND
AFTER EXPOSURE OF THE SAMPLES IN
THE BALLISTIC COMPRESSOR (BC)
(continued)

Sample	No BC	1xBC	2xBC	3xBC
Bi #10	105/104/105			
	101/104/102 102/104/105 103/105			

Typical graphs obtained in the resistance measurements of sample Bi #1 are shown in Figure 20.

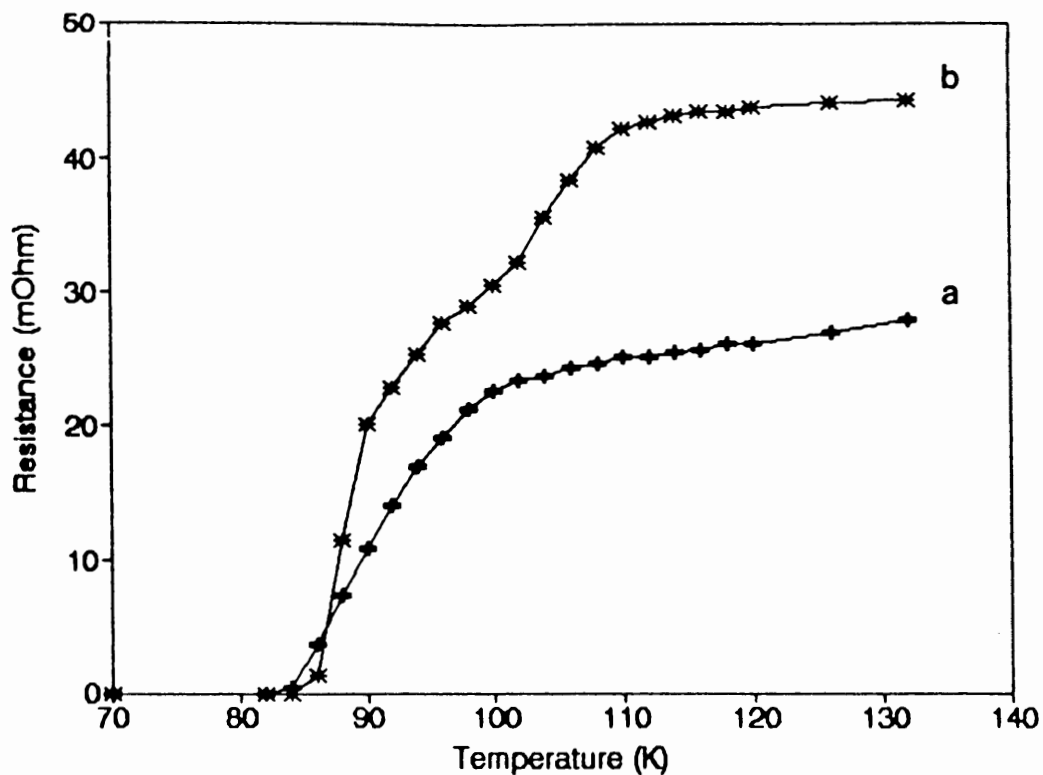


Figure 20. Resistance of sample Bi #1 vs. temperature before (a) and after triple exposure (b) in the ballistic compressor.

Worth mentioning is the two step transition which is only observed in the specimens after exposure in the ballistic compressor.

A two-step superconducting transition was also reported by Yoshimura, *et al.* [14], after reheating a specimen at 1153K. Pissas, *et al.* [6] observed similar transitions in samples of the same composition as in the present work, after annealing at temperatures of up to 875 °C.

TABLE XVI

T_c MEASUREMENTS BY FOUR-POINT PROBE METHOD AT SAMPLE Bi #7
AFTER SINGLE EXPOSURE IN THE BALLISTIC COMPRESSOR
AT DIFFERENT VOLTAGES AND CURRENTS

Max. Voltage	Const. Current	T_c Values
5 V	15 mA	104 K / 105 K
5 V	20 mA	103 K / 103 K
10 V	15 mA	106 K / 106 K
10 V	20 mA	105K / 103K / 104K
40 V	30 mA	103K / 104K / 108K

Conclusions

A uniform dependence on applied voltage or current could not be proved by the results in Table XVI.

The results, shown in Table XV, vary greatly, especially between different experimental runs. Sample Bi #7 showed stable results before exposure in the ballistic compressor. After exposure in the ballistic compressor the T_c values

changed from one day to the other by 20 K (compare sample Bi#7, 1xBC, Table XV with the results in Table XVI; the data were taken on two consecutive days). After the second exposure in the ballistic compressor the sample showed the highest T_c values on the unexposed side. The critical temperature of sample Bi #9 dropped by 15 K in two experimental runs, conducted in exactly the same way.

Different results on different days are possibly an indication for the chemical instability of the samples.

The large variations may also be caused by the inhomogeneity of the samples. It was shown by EDS analysis that the specimens are inhomogeneous in chemical composition. Duan, *et al.* [17] reported about differences in T_c , depending on the direction in which the contacts were aligned. A possible explanation for such a phenomenon is that the pellets are inhomogeneous.

According to Buckel [36], the four-point probe method is not applicable to inhomogeneous specimens. A single continuous superconducting path between the two voltage contacts possibly short-circuits the remaining part of the material, and keeps the voltage down to "zero-voltage", although parts of the volume of the sample are already in the normal conducting state.

Green, *et al.* [11] reported that the high- T_c phase "seems to occur in unconnected regions of the sintered polycrystalline samples, separated by a lower T_c phase".

De Ninno, *et al.* [37] reported about thin insulating layers between two superconducting phases with different T_c within Bi compound bulk specimens.

Jasiolek, *et al.* [7] also showed the inhomogeneity of Bi-Pb-Sr-Ca-Cu-O samples. In their work, EDS analysis revealed a different composition for some small regions of the ceramic material.

FLUX-TRAPPING MEASUREMENTS

Theory

Bi-Pb-Sr-Ca-Cu-O superconductors are Type II superconductors. Type II superconductors are characterized by the phase diagram, shown in Figure 21, and the magnetization curves, shown in Figure 22, where curve (a) refers to an ideal Type II superconductor, while curve (b) refers to a real Type II superconductor. Type II superconductors have in addition to the Meissner phase below B_{c1} and the normal conducting phase above B_{c2} , a mixed phase, the Shubnikov phase [24]; see Figure 21.

The magnetization of an ideal Type II superconductor, shown in Figure 22 (a), is proportional to the external magnetic field as long as it is lower than B_{c1} . The volume of the superconductor is shielded from the external magnetic field. Above B_{c1} , the mean magnetization decreases with increasing external magnetic field, while the volume part of

the normal conducting phase increases. The normal conducting phase enters along with the magnetic field the volume of the superconductor in the form of vortices, which are oriented parallel to the external magnetic field. At B_{c2} , the superconductor is in the normal conducting state. The magnetization curve of an ideal Type II superconductor, shown in Figure 22 (a), is reversible.

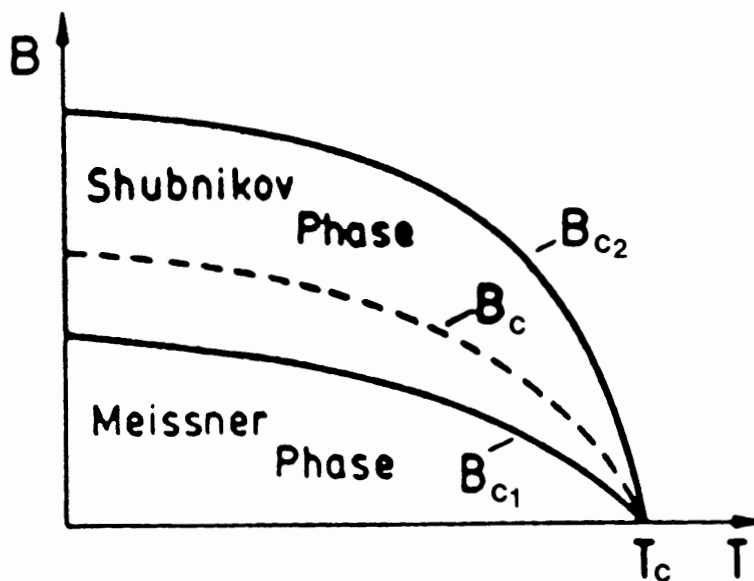


Figure 21. Phase diagram of a Type II superconductor [24].

The magnetization curve of a real Type II superconductor, shown in Figure 22 (b), looks different. Real Type II superconductors have impurities and defects which act pinning centers for the vortices which start penetrating the material at B_{c1} . Since pinning of the vortices to impurities and defects

is energetically favorable, the vortices do not penetrate the whole volume of the material instantly at B_{c1} . Instead, the magnetization of a real Type II superconductor increases with the external magnetic field, even above B_{c1} , to a maximum value which depends on the magnitude of the pinning force. With further increase of the external magnetic field the magnetization decreases; the vortices are arranged in the whole volume of the specimen. At B_{c2} , the superconductor is in the normal conducting state. When the external magnetic field is subsequently lowered to zero, the vortices stick to the pinning centers. At zero external magnetic field the magnetization of the material is different from zero; magnetic flux is "trapped"; see Figure 22 (b).

The idea in the present experiment was to measure the trapped flux in the pellets by means of a Hall probe.

Experiment

The samples were mounted on the end of a piece of stiff tape to handle them when they were submerged in liquid nitrogen. Then they were cooled down in a small thermo-vessel. A magnetic field of about 1.2 Tesla was applied perpendicular to the surface of the pellets and subsequently lowered down to zero. In the phase diagram, shown in Figure 21, this course would be a vertical line, ending on the temperature-axis below T_c . Thereafter, the trapped magnetic field was measured by means of a Hall probe, where two different Models were used.

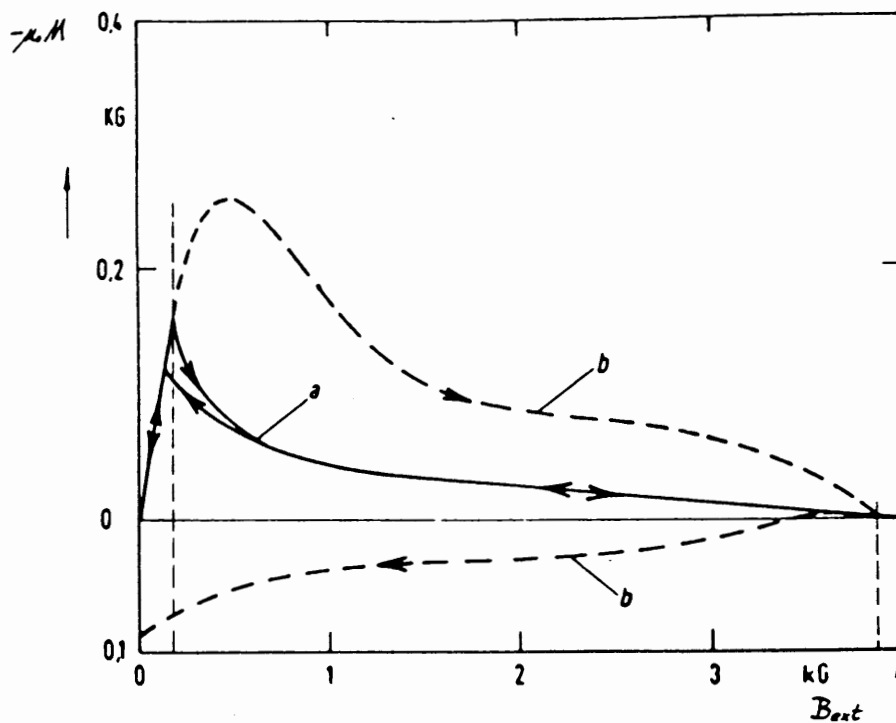


Figure 22. Magnetization of a Type II superconductor [36].

The first instrument was an axial Hall probe (Model A-6011) in connection with a F.W. Bell 620 Gaussmeter. Since this probe was not temperature compensated, the pellets had to be taken out of the thermo-vessel to measure the trapped field. Observable peaks were obtained when the samples were quickly brought near the Hall probe. The peak deflection changed direction when the pellets were turned. The magnetic field decayed fast due to the warming up of the samples in air. Approaching of the probe to a styrofoam cup, which was filled with liquid nitrogen, yields a drop of the detected field of about 1 Gauss. Hence, the detected curves consisted of two effects; the temperature dependence of the Hall probe

yielded a slow decrease in the curve, which was superimposed by sharp peaks due to the trapped flux.

The second instrument was a transverse, cryogenic Hall probe (Model CTP4-3260) connected to the same Gaussmeter. In the experiments with CTP4-3260 both the Hall probe and the pellets were submerged in liquid nitrogen. The actual Hall sensor of the probe was contained in a protecting tube, wherefore the pellets could not be approached directly to the sensor. This resulted in the weakening of the measured magnetic fields by more than a factor of two. Hence, the CTP4-3260 Hall probe had to be calibrated. The instrument was compared to a third Hall probe (Model STB4-0204), which had been calibrated before with a reference magnet. The magnetic field for the calibration was produced by a current in a coil, which had the same diameter as the pellets.

Samples Bi #1 and #7 were measured before and after exposure in the ballistic compressor. The flux trapping capability of both pellets did not change visibly after exposure in the ballistic compressor. The trapped flux of sample Bi #1 was only about 0.06 G, which is about 20 times less than the Earth's magnetic field. Hall probe CTP4-3260 did not give a detectable signal, when measuring flux in sample Bi #1. The maximum trapped magnetic flux in sample Bi #7 was about 0.4 G. Results are shown in Table XVII.

The measured trapped flux is low. However, sharp peaks indicate that the measuring results are due to trapped

magnetic flux in the samples. Inversion of the peaks, when turning the pellets also supports this statement.

The absolute trapped flux in sample Bi #7 (0.8 mm thickness) is about 8 times higher than that in sample Bi #1 (3.2 mm thickness). This is in accordance with the results obtained in the Meissner effect determination. In these experiments, sample Bi #7 showed a stronger deviation of the test-magnet than sample Bi #1. Thinner samples have more defects which are capable of trapping flux.

TABLE XVII

MAXIMUM VALUES OF TRAPPED FLUX IN
SAMPLES Bi #1 and #7 WITH TWO
DIFFERENT HALL PROBES

Sample	Number of Exposures	A-6011	CTP4-3260
Bi #1	No	0.06 G	
	3 x	0.05 G	
Bi #7	No	0.4 G	
	1 x	0.39 G	
	2 x	0.4 G	0.39 G
Bi #8	No	0.5 G	
Bi #10	No	0.45 G	

Findings of Other Researchers

The low current densities in the Bi-Pb-Sr-Ca-Cu-O system, which are connected to the magnitude of the pinning force, can be explained again by the inhomogeneity of the samples.

Laverty, *et al.* [12] reported that the grains of the (2223)

phase are separated by (2212) material so that at liquid nitrogen temperature J_c was zero. This strongly supports the results obtained in this work.

Ninno, *et al.* [37] reported critical current densities J_c lower than 50 A/cm^2 in the system Bi-Sr-Ca-Cu-O, while Vassilev, *et al.* [29] measured critical current densities of 20 - 30 A/cm^2 in the system $\text{Bi}_{2-x}\text{Pb}_x\text{Sr}_2\text{Ca}_2\text{Cu}_3\text{O}_y$. Vassilev ascribes the low current densities to weak-links, mainly consisting of (2212)- and (2201)-phases.

Imanaka, *et al.* [38] reported an enhancement of the critical current density with the decrease of the sample thickness of Bi-Pb-Sr-Ca-Cu-O samples. This is in accordance with the present results, since sample Bi #7 is just 0.8 mm thick compared to sample Bi #1, which is 3.2 mm thick.

CHAPTER V

SUMMARY AND CONCLUSIONS

The effect on samples of nominal composition $\text{Bi}_{1.8}\text{Pb}_{0.2}\text{Sr}_2\text{Ca}_2\text{Cu}_3\text{O}_y$ was investigated when they were exposed to hot, dense argon in a ballistic compressor.

The two samples Bi #1 and #7, on which the investigations were concentrated, show a distinct surface morphology. The surface structure of sample Bi #1 suggests that surface melting covering all areas has occurred, while the surface of sample Bi #7 still shows fragments of the structure before exposure in the ballistic compressor.

X-Ray analysis on both samples confirms that melting with subsequent rapid cooling of the material favors the formation of the high- T_c (2223) phase.

It was shown by EDS analysis that the samples are inhomogeneous in chemical composition. Exposure of the samples in the ballistic compressor results in an increase in the amount of Sr on the surface. Oxygen loss, due to exposure in the ballistic compressor, could not be proved clearly.

Varying T_c values obtained by the four-point probe method also indicate inhomogeneity of the samples. More appropriate measuring methods, which do not require homogeneous samples, could probably give more reliable results.

In both samples, only small amounts of trapped flux which are related to the low critical current densities, were measured. Low critical current densities were reported by [12,29,37]. The separation of the high- T_c (2223) phase by other phases, present in the multiphase compound, might be the reason for low critical current densities at liquid nitrogen temperature.

Sample Bi #7 traps a higher amount of flux and shows stronger absolute Meissner effect than sample Bi #1. However, ballistic compressor exposure of sample Bi #7 did not improve its properties, whereas sample Bi #1 shows an increase in Meissner effect on the exposed side, after triple exposure in the ballistic compressor. The trapped flux in sample Bi #1 was too weak to be detected by the cryogenic Hall probe CTP4-3260.

REFERENCES

1. Bednorz, J. & Müller, K. Z. Phys. B **64**, 189 (1986).
2. Wu, M., Ashburn, J., Torng, C., Hor, P., Meng, R., Gao, L., Huang, Z., Wang, Y., & Chu, C. Phys. Rev. Lett. **58**, 908 (1987).
3. Michel, C., Hervieu, M., Borel, M., Grandin, A., Deslandes, F., Provost, J., & Raveau, B. Z. Phys. B **68**, 421 (1987).
4. Maeda, H., Tanaka, Y., Fukutomi, M., & Asano, T. Jpn. J. Appl. Phys. **27**, L209-L210 (1988).
5. Tarascon, J., McKinnon, W., Barboux, P., Hwang, D., Bagley, B., Greene, L., Hull, G., LePage, Y., Stoffel, N., & Giroud, M. Phys. Rev. B **38**, 8885-8892 (1988).
6. Pissas, M., Niarchos, D., Christides, C., & Anagnostou, M. Supercond. Sci. Technol. **3**, 128-133 (1990).
7. Jasiulek, G., Gorecka, J., Majewski, J., Yuan, S., Jin, S., & Liang, R. Supercond. Sci. Technol. **3**, 194-198 (1990).
8. Maeda, A., Hase, M., Tsukada, I., Noda, K., Takebayashi, S., & Uchinokura, K. Phys. Rev. B **41**, 6418 (1990).
9. Tallon, J., Buckley, R., Gilberd, P., Presland, M., Brown, I., Bowden, M., Christian, L., & Goguel, R. Nature **333**, 153-156 (1988).
10. Cava, R. & et al. Physica C **153-155**, 560-565 (1988).
11. Green, S., Jiang, C., Mei, Y., Luo, H., & Politis, C. Phys. Rev. B **38**, 5016-5018 (1988).
12. Laverty, J., Caplin, A., & Male, S. Physica C **162-164**, 1165-1166 (1989).
13. Tomy, C., Prasad, R., Soni, N., Adhikary, K., Gulnar, A., & Malik, S. Physica C **162-164**, 925-926 (1989).
14. Yoshimura, M., Sung, T., Nakagawa, Z., & Nakamura, T. J. Mat. Sci. Letters **8**, 687-688 (1989).

15. Dash, J., Takeo, M., Trzynka, A., Roush, J., Kasaaian, A., Brace, F., Takeo, H., & Weaver, P., in Metallurgical Applications of Shock-Wave and High-Strain-Rate Phenomena, 61 (ed. Murr, L., Staudhammer, K., & Meyers, M.) 1051-1069 (Marcel Dekker, Inc., New York and Basel, 1986).
16. Sunshine, S. & et al. Phys. Rev. B **38**, 893 (1988).
17. Duan, Q. & Dash, J. Proceedings of the XIIth International Congress for Electron Microscopy, 90-91 (1990). (San Francisco Press, Inc., San Francisco)
18. Duan, Q., Dash, J., Takeo, M., & Huang, J. J. Appl. Phys. **69** (8), 4897-4898 (1991).
19. Ichinose, N. Personal Communication (1992). (Waseda University, Tokyo)
20. Takeo, M., Holmes, Q., & Ch'en, S. J. Appl. Phys. **38** (9), 3544-3550 (1967).
21. Holmes, R., Ch'en, S., & Takeo, M. JOSRT **9**, 249 (1968).
22. Takeo, M. Personal Communication (July 1992). (Portland State University)
23. Duan Q. Personal Communication (1992). (Portland State University)
24. Kopitzki, K. Einführung in die Festkörperphysik, 1989 (Teubner Studienbücher, Stuttgart, 1989).
25. Meissner W. & Ochsenfeld, R. Naturwissenschaften **21**, 787 (1933).
26. Powers, M. Proceedings of the XIIth International Congress for Electron Microscopy, 66-67 (1990). (San Francisco Press, Inc., San Francisco)
27. Watt, I. The principles and practice of electron microscopy, 1989, 33 (Press Syndicate of the University of Cambridge, Cambridge, 1985).
28. Johnson Jr., G. & White, E. X-Ray Emission Wavelengths and KeV Tables for Nondiffractive Analysis, ASTM DATA Services DS 46 (American Society for Testing and Materials, Philadelphia, 1970).
29. Vassilev, P., Mateev, M., Mikhov, M., Kovacheva, D., Petrov, K., & Kovachev, V. Physica C **162-164**, 917-918 (1989).

30. Nagoshi, M. & Suzuki, T. Phys. Rev. B **43**, 10445-10450 (1991).
31. Peuckert, M., Becker, W., Bock, J., Hettich, B., Neumüller, H., & Schwarz, M. Physica C **162-164**, 893-894 (1989).
32. Duan, Q. ESR Seminar (June 4, 1992). (Portland State University)
33. Hirsch, P., Howie, A., Nicholson, R., Pashley, D., & Whelan, M. Electron Microscopy of Thin Crystals, 536 (Plenum Press, New York, 1965).
34. Bartram, S. Handbook of X-Rays (ed. Kaelble, E.) 17-1 (McGraw-Hill Book Company, New York, San Francisco, Toronto, London, Sydney, 1967).
35. Bragg, L. The Crystalline State, 1955 (ed. Sir Lawrence Bragg) 189 (G. Bell And Sons LTD, London, 1933).
36. Buckel, W. Supraleitung, 1990 (VCH, Weinheim, Basel, 1972).
37. De Ninno, A., Gislou, P., Marinelli, M., Paterno, G., Gambardella, U., Paroli, P., & Balestrino, G. Physica C **162-164**, 359-360 (1989).
38. Imanaka, N., Imai, H., & Adachi, G. Jpn. J. Appl. Phys. **28**, L2158-L2160 (1989).